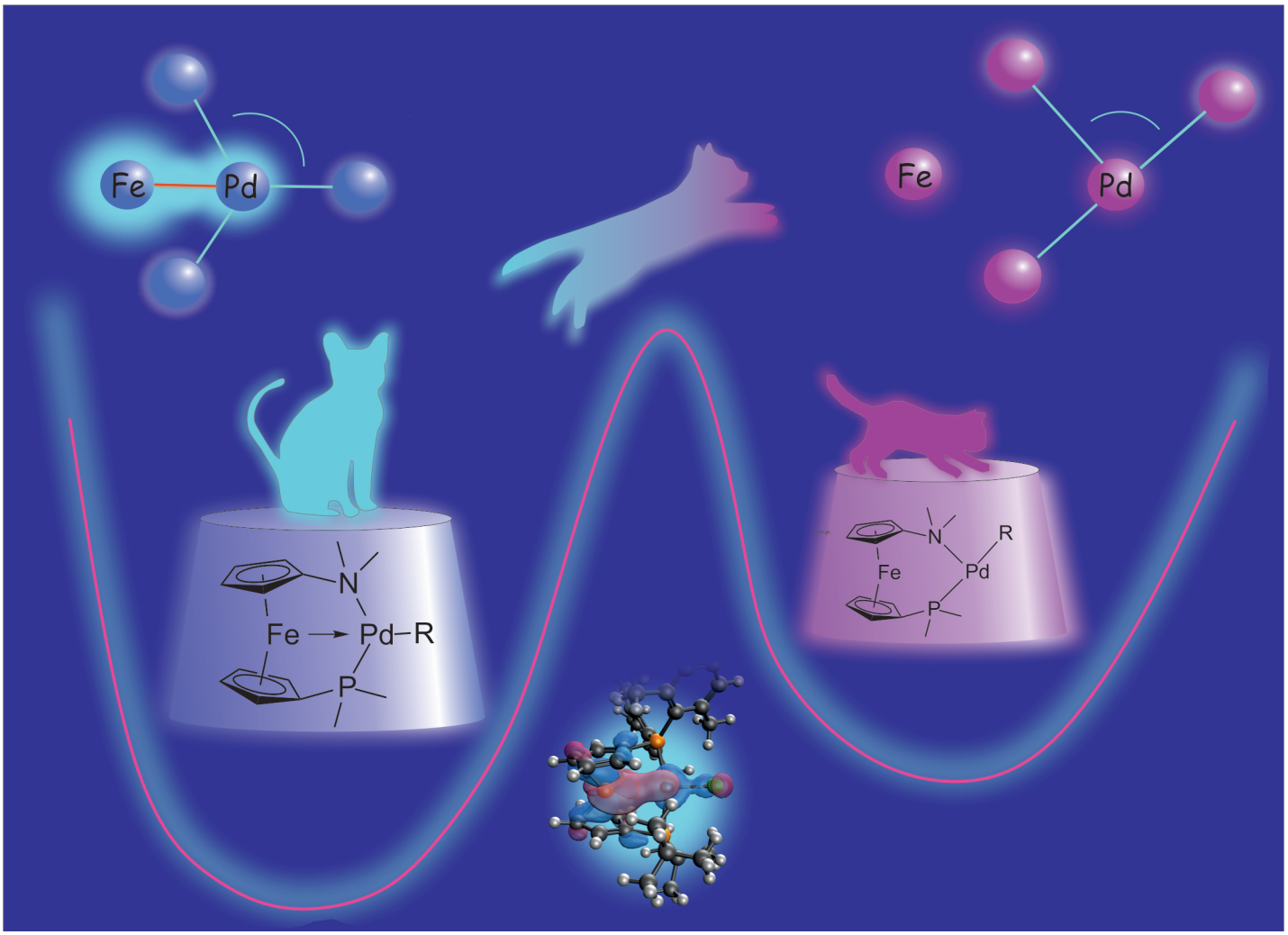

Showcasing research from the groups of Rudolf Pietschnig at the University of Kassel, Germany and Zsolt Kelemen at the Budapest University of Technology and Economics, Hungary.

Tailoring the Fe → Pd interaction in cationic Pd(II) complexes *via* structural variation of the ligand scaffold of sterically demanding dppf-analogs and their P,N-counterparts

Ferrocene-based P,N and P,P ligands are presented with their cationic Pd(II) complexes featuring examples with the shortest or longest Fe-Pd distances reported so far compared with related ligands, and the underlying Fe → Pd interaction is analyzed with DFT calculations.

As featured in:

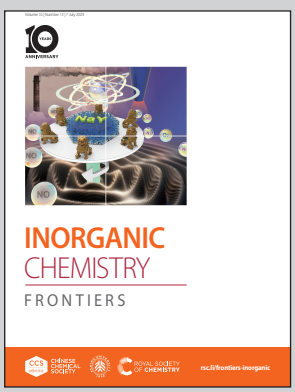

See Zsolt Kelemen, Rudolf Pietschnig *et al.*, *Inorg. Chem. Front.*, 2023, **10**, 3828.

CCS 中国化学会 CHINESE CHEMICAL SOCIETY
PEKING UNIVERSITY 1898
ROYAL SOCIETY OF CHEMISTRY
rsc.li/frontiers-inorganic

INORGANIC CHEMISTRY
FRONTIERS

RESEARCH ARTICLE

View Article Online
View Journal | View Issue

Cite this: *Inorg. Chem. Front.*, 2023, **10**, 3828

Tailoring the Fe → Pd interaction in cationic Pd(II) complexes *via* structural variation of the ligand scaffold of sterically demanding dppf-analogs and their P,N-counterparts†‡

Subhayan Dey,[a] Fabian Roesler,[a] Clemens Bruhn,[a] Zsolt Kelemen *[b] and Rudolf Pietschnig *[a]

Two 1,1′-azaphospha substituted dppf-analogues Fc′(NMe_2)(PPh_2) (Ph = C_6H_5, Fc′ = 1,1′-ferrocenediyl, **3a**) and Fc′(NMe_2)($PMes_2$) (Mes = 2,4,6-$Me_3C_6H_2$, **3b**) have been prepared, *via* reductive amination, followed by salt-metathesis (of **2**), starting from 1,1′-azabromoferrocene **1**. Their donor properties have been explored using heteronuclear NMR spectroscopy based on their $^1J_{P-Se}$ coupling, and the formation of $PdCl_2$-complexes in comparison to a set of related dppf analogs with gradual steric variation, such as Fc′($PMes_2$)(PPh_2) (**5**) and Fc′($PMes_2$)(P^tBu_2) (**6**). Chloride abstraction from these complexes, namely Fc′($PMes_2$)(PPh_2)·$PdCl_2$ (**7**), Fc′($PMes_2$)(P^tBu_2)·$PdCl_2$ (**8**), and [Fc′(NMe_2)(PPh_2)]$_2$·$PdCl_2$ (**9**) using $AgSbF_6$ produced the corresponding cationic Pd(II) complexes [Fc′($PMes_2$)(P^tBu_2)·PdCl][SbF_6] (**10**), [Fc′(PPh_2)(NMe_2)·PdCl][SbF_6]$_2$ (**11**) and [Fc′(PPh_2)(NMe_2)·Pd($PPh_2C_5H_5$)]][SbF_6]$_2$ (**12**) featuring Fe → Pd interactions. Variation of the counter anion by coordination of **3a** to a chloride-free Pd(II) source furnished [Fc′(PPh_2)(NMe_2)·Pd(PPh_3)][BF_4]$_2$ (**13**), [Fc′(PPh_2)(NMe_2)·Pd(PPh_2)Fc′(NMe_2)][BF_4]$_2$ (**14**), and [Fc′(PPh_2)(NMe_2)·PdP(*p*-OMe-C_6H_4)$_3$][BF_4]$_2$ (**15**) with similar Fe → Pd interactions. Comparison with previously reported diphospha- and azaphospha- counterparts, revealed that **10** and **11** display the shortest and **15** the longest Fe–Pd bond, within their ligand scaffold congeners. DFT calculations performed on compounds **10–15** were further able to verify their intrinsic structural features and trends and shed light on the nature of the Fe → Pd bonding interactions which are furthermore consistent with CV measurements.

Received 29th March 2023,
Accepted 28th April 2023

DOI: 10.1039/d3qi00576c

rsc.li/frontiers-inorganic

Introduction

Ferrocene, an extremely useful and unique building block, has remained at the centre of attraction for several decades now.[1,2] Being an essential component in organometallic polymers,[3–10] redox-tunable substances,[6,11–13] organometallic drugs,[14,15] and functional materials,[9,16–20] ferrocene has played a vital role in homogenous catalysis.[21–25] The principle reasons for its popularity in homogenous catalysis lie in the easy syntheses of its P-functionalized derivatives (such as dppf) and a flexible backbone,[26,27] which provides an opportunity to stabilize various metal centers by attaining facile geometric changes.[21,28] When such ferrocene-based ligands were further explored in respect to catalysis, it was found that bite angles (β_n) of such ligands, which have a positive effect on the efficiency of catalysts,[29,30] are significantly higher than those found for usual bisphosphanyl ligands (such as dppe),[29–31] and can further be manipulated by changing the substituents on phosphorus.[27] These aforementioned qualities made ferrocene-based bisphosphane ligands remarkably successful,[21,22] and a search for new ligands, with optimized steric demand and donating ability, is still relevant to date.[32–37]

Analogous heteroditopic P,N-ligands with a 1,1′-backbone are far less explored (type **E**, Fig. 1), unlike other heteroditopic amino ferrocene ligands (**B–D**, Fig. 1).[33,54,66–69,71] The simultaneous presence of P and N donor atoms in a single molecule, are attractive to differentiate between their softness according to the HSAB concept and to foster hemilabile coordination. Recently the chemistry of κ^3-bis(donor)ferrocenyl – transition-metal interactions has been reviewed as well.[72]

Here we report a general approach to ferrocene bridged 1,1′-disubstituted P,N-ligands of the general type **E** and explore

[a]*Institut für Chemie und CINSaT, University of Kassel, Heinrich Plett-Straße 40, 34132 Kassel, Germany. E-mail: pietschnig@uni-kassel.de*
[b]*Department of Inorganic and Analytical Chemistry, Budapest University of Technology and Economics, Műegyetem Rkp. 3, 1111 Budapest, Hungary*

†Dedicated to Prof. Dr László Nyulászi on the occasion of his 65th birthday.

‡Electronic supplementary information (ESI) available: Synthetic protocols, NMR spectra, crystal refinement data, CV and details of DFT calculations. CCDC 217930 and 2243451–2243462 for compounds **1**, **3b**, **4a**, **7–15**, respectively. For ESI and crystallographic data in CIF or other electronic format see DOI: https://doi.org/10.1039/d3qi00576c

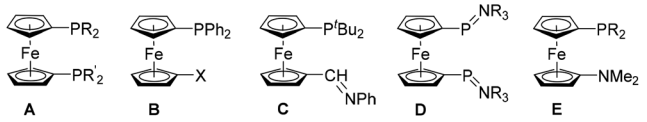

Fig. 1 Previously reported symmetrically and unsymmetrically substituted dppf-analogs (**A–D**), and herein reported 1,1′-azaphospha substituted ferrocenyl ligands (**E**, R = Ph, Mes). Known 1,1′-diphospha substituted dppf-analogues **A**: R = R′ = Ph, Mes, ^{t}Bu *etc.*;[23,27,32,38–48] 1,1′-unsymmetrically substituted diphenylphosphano ferrocenes **B**: X = CHO,[49,50] COOH,[51] COOMe,[51] $CONEt_2$,[52] $C{=}CBr_2$,[49] C≡CH,[49] $HC{=}CH_2$,[53] C≡N,[54] CH_2OH,[34] SH,[55] oxazoline,[56] $PO(OEt)_2$,[57] COOH,[58,59] OMe,[60] C_5H_4N,[61] bipyridine,[62] $HC{=}N(C_6F_5)$,[63,64] $CH_2NH(CHMePh)$,[50] CHN(CHMePh),[50] 3,5-dihydroazepine,[65] N≡C,[54] N=C(NH^{i}Pr)$_2$,[66] N=C(NHC$_6$H$_{11}$)$_2$,[66] N=C(NHXyl)$_2$,[66] $NH(CO)CH_2PPh_2$,[67] and $NH(CH_2)_2PPh_2$;[67] 1,1′-unsymmetrically substituted di-*tert*-butylphosphano ferrocenes **C**;[68,69] and bis(phosphinimine) ligands **D**: R = Et and Ph.[70] Analogous heteroditopic P,N-ligands, presented in this report, **E**: R = Ph and Mes.

their donor properties. Furthermore, we apply these dppf analogous P,N and closely related P,P ligands in the coordination of Pd(II) ions where depending on the counter-anions a gradual tuning of Fe → Pd interactions is achieved which besides structural investigation is explored with density functional theory (DFT) and electrochemical methods (CV).

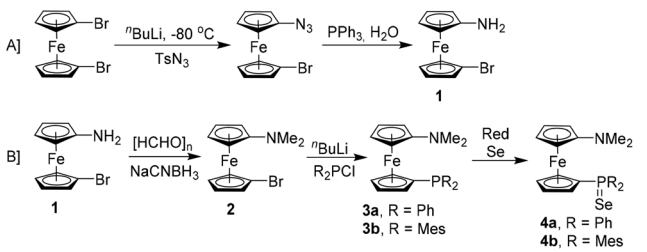

Scheme 1 Synthesis and preliminary reactions of compound **3** and its derivatives.

Results and discussion

Synthesis and properties of ferrocene bridged P,N-ligands

Whereas all previously reported azaphospha-substituted ferrocene ligands have been synthesized starting from BH_3-protected ferrocenyl phosphanes,[33,54,67,71] the synthesis of azaphosphanes **3** (with generic structure of **E**, depicted in Fig. 1) hinges upon successful and large-scale preparation of an unsymmetrically substituted 1,1′-azabromoferrocene **1**. Although there are several synthetic strategies reported for compound **1**,[73–77] due to low obtainable yields,[73,75–77] and apparently impure final product,[73,74,76,77] a newly reported pathway, which involves Staudinger-type reaction on 1,1′-azidobromoferrocene (Scheme 1A),[78] was used for this compound. Compound **1** was initially purified by column chromatography, followed by a flask-to-flask sublimation, which resulted in bright colored golden yellow crystals, which were found suitable for characterization by single crystal X-ray diffraction (Fig. 2 and S2, ESI‡).

Adapting a known procedure for reductive amination on aminoferrocenes,[77,79,80] compound **1** was further reacted with paraformaldehyde and $NaCNBH_3$, in presence of glacial acetic acid to obtain *N*,*N*-dimethyl substituted 1,1′-azabromoferrocene **2** (Scheme 1B). When compound **2** was lithiated and *in situ* reacted with one equivalent of Ph_2PCl or Mes_2PCl, compound **3a** and **3b** were obtained in yields of 69% and 21%, respectively, calculated based on starting material **1** (Scheme 1B). Although the crystal structure of compound **3a** was deposited in 2003 by Butler *et al.* (CCDC Deposition Number 217930‡, deposited on 07/10/2003),[81] no further report, describing its synthesis and characterization, could be

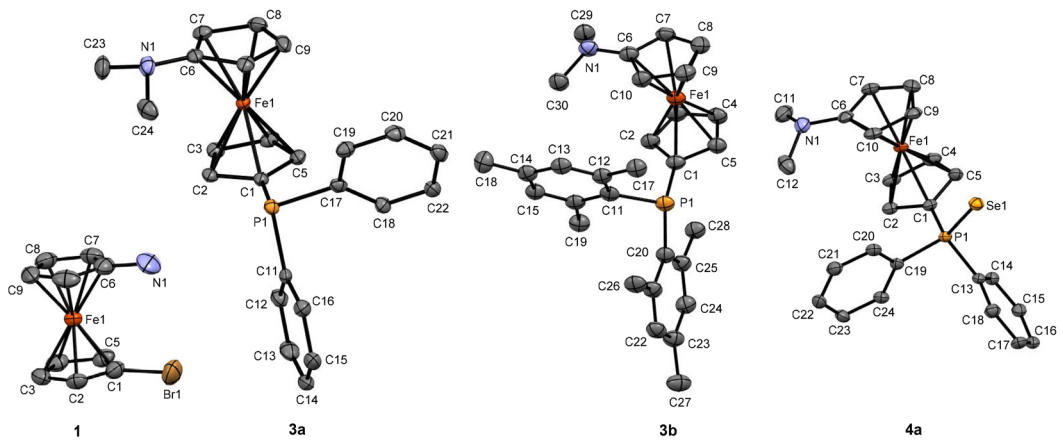

Fig. 2 Ortep plot of the molecular structures of **1**, **3a**, **3b** and **4a** in the solid state with ellipsoids drawn at the 50% probability level, where H atoms are omitted for clarity. Selected bond lengths [Å] and angles [°] for **1**: N1–C6 1.477(6), Br1–C1 1.883(4), C7–C6–N1 127.2(5), C5–C1–Br1 126.0(3). Selected bond lengths [Å] and angles [°] for **3a**, **3b** and **4a**: N1–C6 1.391(4) for **3a**, and 1.386(4) for **3b**, and 1.389(4) for **4a**; P1–C1 1.814(3) for **3a**, 1.813(3) for **3b** and 1.788(3) for **4a**; *ipso*C^{Aryl}–P–*ipso*C^{Cp} 101.63(12) and 102.64(12) for **3a** (where Cp denotes the C_5H_4 moiety of substituted ferrocene), 101.72(13) and 109.10(13) for **3b**, 104.87(12) and 104.00(13) for **4a**; *ipso*C^{Aryl}–P–*ipso*C^{Aryl} 98.98(12) for **3a**, 105.18(13) for **3b**, and 104.42(12) for **4a**.

found despite our best effort. Therefore, synthetic details and complete characterization of compound **3a** are presented in this report, whereas an independently developed crystallographic data set, obtained by X-ray analysis from a single crystal of **3a**, was used for further discussion.

Although the solid-state molecular structures of **3a** and **3b** are very similar, their geometries at the phosphanyl unit differs owing to the different steric demand of the P-bonded substituents, with the sum of angles at phosphorus being larger by *ca.* 13° in mesityl substituted **3b** than in phenyl substituted **3a** (Fig. 2). This observation is consistent with related sterically demanding dppf analogs, Fc′($PMes_2$)(PPh_2) and Fc′($PMes_2$)$_2$,[82,83] for which better donor ability has been found for Mes_2P- than for Ph_2P- groups, based on variation of the s-character of the lone pair at phosphorus with the geometry at this atom.[23,82,83]

To examine how the diarylphosphanyl groups in **3a** and **3b** are influenced by the amino unit in the molecule, we set out to determine the $^1J_{P–Se}$ values as a measure for their donating properties. To this end, **3a** and **3b** were reacted with red selenium forming selenophosphoranes **4a** and **4b** (Scheme 1B) featuring $^1J_{P–Se}$ coupling values of 757 Hz and 719 Hz (in Toluene-D8), respectively, which are *ca.* 4–6 Hz lower than those reported for Fc′($PSePh_2$)$_2$ (761 Hz), Fc′($PSeMes_2$)($PSePh_2$) (763^{PSePh2} and 723^{PSeMes2} Hz), and Fc′($PSeMes_2$)$_2$ (723 Hz) in the same solvent.[23,82] The lower values for $^1J_{P–Se}$ in **4a** and **4b** indicate a better donor ability of the phosphanyl units as compared to their counterparts without the NMe_2 unit. Moreover, by careful evaluation of the structure of **4a** (Fig. 2), its molecular parameters were found in compliance with the comparable values of Fc′($PSeMes_2$)($PSePh_2$) and Fc′($PSePh_2$)$_2$.[83,84] To explore the overall electronic effect of simultaneous introduction of NMe_2 and PR_2 (R = Ph and Mes) units in this molecular scaffold, the redox properties of the metallocene units **3a** and **3b** have further been investigated using cyclic voltammetry (CV, Fig. S1, ESI‡), where the introduction of NMe_2 unit shows a significant shift of Fc/Fc^+ oxidation maxima (133 and 26 mV for **3a** and **3b**, respectively, where Fc denotes ferrocene) towards lower potentials, as compared to $FcPPh_2$ and $FcPMes_2$, respectively (Fig. S1, ESI‡).

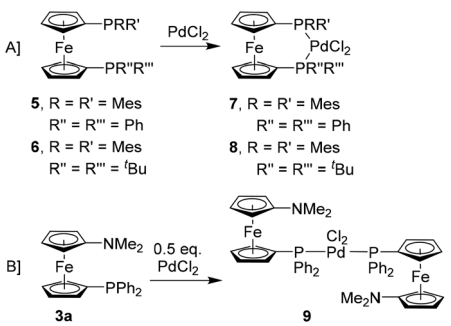

Scheme 2 Synthesis of $PdCl_2$ complexes of ligands **3a**, **5** and **6**.

Pd(II) complexes of Dppf-analogs

For mutual comparison, $PdCl_2$ complexes of P,N ligand **3a** and P,P ligands **5** and **6** have been prepared in dichloromethane by adapting a published procedure (Scheme 2).[28,41,85] The ^{31}P NMR resonances of the donor atoms in bisphosphane ligands **5** and **6** experience significant deshielding upon conversion into their respective $PdCl_2$ complexes **7** and **8** with coordination shifts of $\Delta\delta \approx 50$ ppm. By contrast, the corresponding P, N ligand **3a** shows no significant shift of its ^{31}P resonance upon coordination in **9**. The closely related mesityl substituted **3b** did not undergo complex formation with $PdCl_2$ in CH_2Cl_2 solution at room temperature, whereas at higher temperature in toluene solution unspecific reaction led to inseparable mixtures (Fig. S59 and S60, ESI‡).

Single crystals, suitable for X-ray crystallography, could be obtained by slow diffusion of hexanes or pentane into solutions of complexes **7**–**9** in dichloromethane revealing bidentate coordination of the P,P ligands in **7** and **8** in contrast to monodentate coordination of the P,N ligand in **9** (Fig. 3).

To increase the metal ligand interaction, complexes **7**–**9** were further reacted with $AgSbF_6$ as chloride abstracting

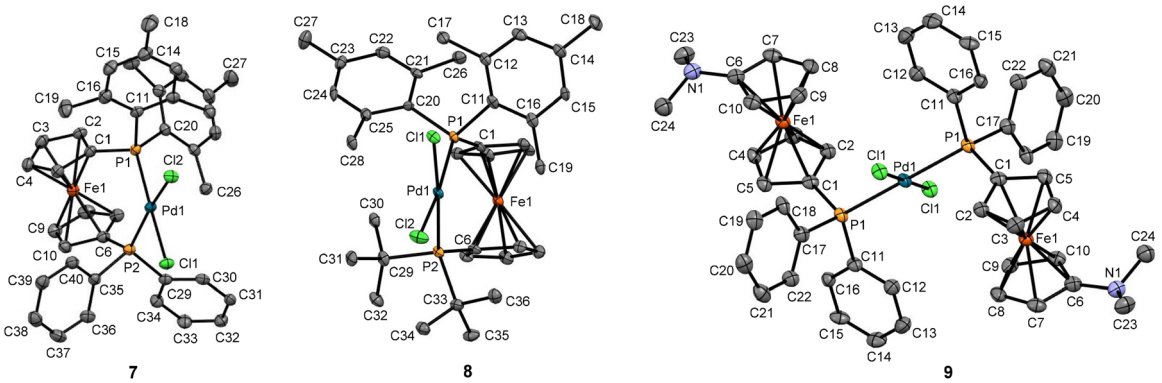

Fig. 3 Ortep plots of the molecular structures of **7**–**9** in the solid state with ellipsoids drawn at the 50% probability level, where H atoms, solvent molecules, and labels for a few atoms are omitted for clarity. Selected bond lengths [Å] and angles [°] for **7**–**9**: P1–Pd1 2.3470(6) (**7**), 2.3167(13) (**8**), 2.3361(17) (**9**); P2–Pd1 2.2899(6) (**7**), 2.3518(13) (**11**); Pd1–Cl1 2.3599(6) (**7**), 2.3792(12) (**8**), 2.2933(18) (**9**); C1–P1 1.812(2) (**7**), 1.835(5) (**8**), 1.789(6) (**9**); P1–Pd1–P2 101.73(2) (**7**), 103.37(5) (**8**); P1–Pd1–P1′ 180.0.

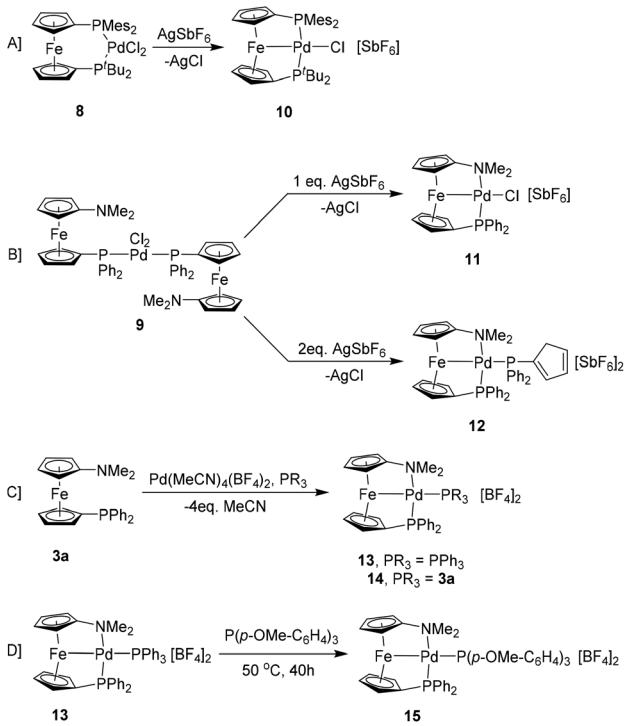

Scheme 3 Synthesis of Pd(II) complexes of dppf analogs with Fe → Pd Interactions.

reagent (Scheme 3). In case of complex **7**, the all aryl substituted P,P ligand experiences irreversible oxidation leading to insoluble paramagnetic products. By contrast, chloride abstraction from complex **8** leads to formally cationic Pd-complex **10** with the P,P ligand remaining intact (Scheme 3A). For Pd complex **9**, containing P,N ligand **3a** in monodentate fashion, the reaction depends strongly on the stoichiometry of the reagents. For sub-stoichiometric and stoichiometric amounts of $AgSbF_6$, chloride abstraction is successful and the twofold monodentate binding mode changes to bidentate with elimination of the second equivalent of ligand leading to **11** (Scheme 3B). With excess (2 eq.) of $AgSbF_6$ a similar hapticity change of the P,N ligand occurs, however, both chloride ions are removed to form dicationic complex **12** (Scheme 3B). Within the latter, the coordination sphere around palladium is completed by cyclopentadienyl diphenylphosphane, which we anticipate stemming from fragmentation of the second ligand unit in **9** (Scheme 3B). A similar bidentate and dicationic complex **13** can be obtained directly starting from P,N ligand **3a** by reaction with $Pd(NCCH_3)_4(BF_4)_2$ as palladium source in the presence of PPh_3 (Scheme 3C). In the absence of an additional phosphane ligand, or in the presence of sterically very demanding phosphanes (*e.g.*, P(*o*-tol)$_3$ or $PMes_3$), complex **14** is formed, where the second equivalent of ligand in the precursor acts as additional phosphane (Scheme 3C). Moreover, one might speculate about a potential role of **14** as precursor in the formation of **12**. Interestingly, the additional phosphane ligand can be displaced within the ligand sphere of Pd as has been demonstrated by displacement of PPh_3 by P(*p*-anisyl)$_3$ yielding **15** (Scheme 3D). Similar phosphane displacement has been previously reported, which underwent much faster (reaction time 5 min),[86] whereas displacement of PPh_3 by P(*p*-OMe-C_6H_4)$_3$ to **15** took longer time and higher reaction temperature (40 h, 50 °C) as followed by ^{31}P NMR spectroscopy (Fig. S64–S67, ESI‡).

In their ^{31}P NMR spectra the cationic Pd complexes **11–15** related to the P,N ligand show a coordination shift to lower field of roughly $\Delta\delta \approx 12$ ppm *versus* their neutral counterpart **9**. By contrast, with the P,P ligand a significantly larger high-field shift is observed for cationic complex **10**, compared with its neutral precursor **8**, which is more pronounced for the mesityl substituted phosphanyl unit ($\Delta\delta$ = −63.6 ppm) than for the *tert*-Butyl substituted one ($\Delta\delta$ = −51.3 ppm). For completeness, it needs to be mentioned that the sterically more demanding P,N ligand **3b** does not form analogous Pd(II) complexes even with $Pd(NCCH_3)_4(BF_4)_2$ as palladium source (Fig. S58, ESI‡).

We have been able to grow crystals suitable for single crystal X-ray diffraction for **10–15**. For all cationic complexes (**10–15**), a bidentate coordination of one ferrocenylene bridged ligand is observed and a short contact between iron and palladium, which was absent in their neutral precursors **7–9** (Fig. 3, 4 and 5). In general, no direct interaction of the complex counter-anions (BF_4^-, SbF_6^-) with the Pd atom is present which also show no significant effect on the overall structure of their corresponding cations.

When analyzing and discussing the lengths of Fe–Pd distances for these complexes, one has to keep in mind that the difference in $C^{ipso,Cp}$–P or $C^{ipso,Cp}$–N bond lengths also affects the respective Fe–Pd distances and interactions for related diphospha- and diaza-substituted dppf analogs. Therefore, shorter Pd–Fe distances are to be expected for ferrocene based

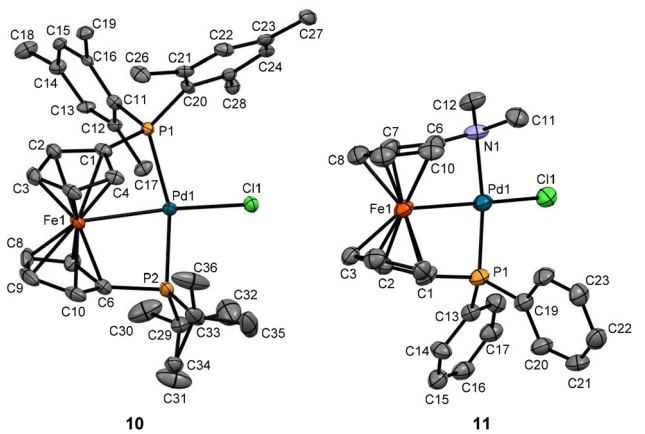

Fig. 4 Ortep plots of the molecular structure of **10** and **11** in the solid state with ellipsoids drawn at the 50% probability level, where H atoms, anions (SbF_6^-) and solvent molecules are omitted for clarity. Selected bond lengths [Å] and angles [°]: P1–C1 1.785(5) (**10**), 1.783(11) (**11**); P1–Pd1 2.3404(14) (**10**), 2.190(3) (**11**); Fe1–Pd1 2.8369(10) (**10**), 2.7384(18) (**11**); Pd1–P2 2.2751(16) (**10**); P2–C6 1.792(5) (**10**); N1–C6 1.394(15) (**11**); C1–P1–Pd1 82.94(17) (**10**), 92.6(3) (**11**); P1–Pd1–Fe1 82.29(4) (**10**), 82.35 (8) (**11**); P2–Pd1–P1 161.60(5) (**10**); N1–Pd1–P1 163.9(2) (**11**).

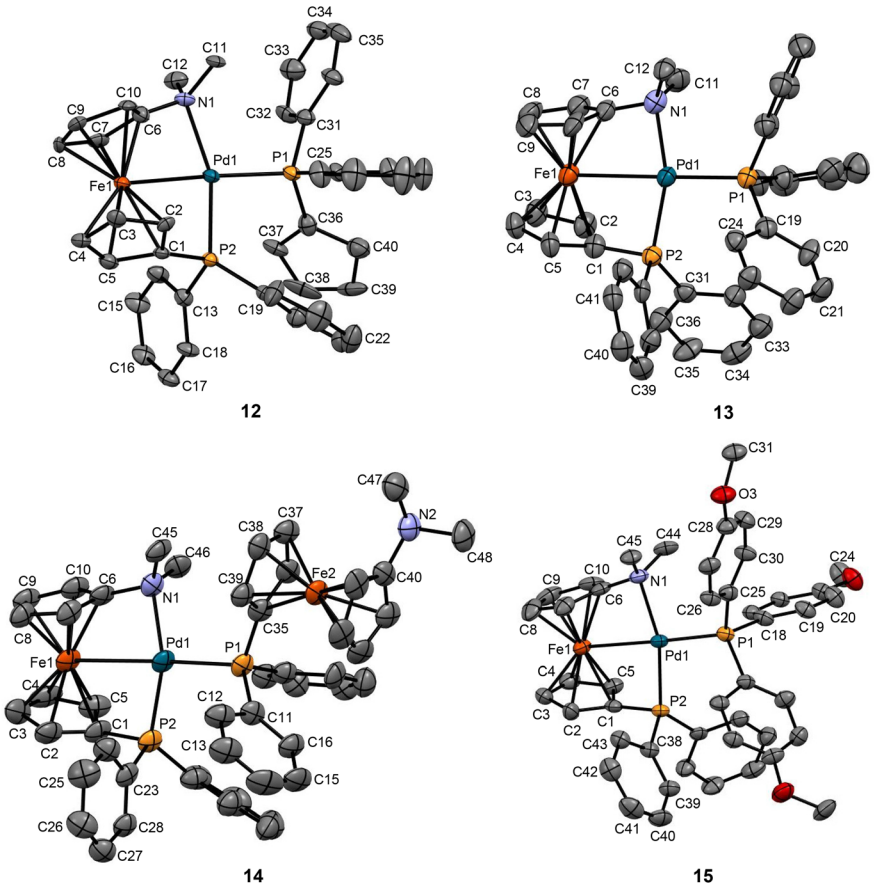

Fig. 5 Ortep plots of the molecular structures of **12–15** in the solid state with ellipsoids drawn at the 50% probability level, where H atoms, anions (SbF_6^- for **12** and BF_4^- for **13–15**), solvent molecules and labels for a few atoms are omitted for clarity. Selected bond lengths [Å] and angles [°]: N1–C6 1.420(9) (**12**), 1.415(12) (**13**), 1.427(7) (**14**), 1.408(9) (**15**); C1–P2 1.788(8) (**12**), 1.758(10) (**13**), 1.766(6) (**14**), 1.770(7) (**15**); Pd1–N1 2.150(6) (**12**), 2.123 (8) (**13**), 2.138(5) (**14**), 2.146(5) (**15**); Pd1–P2 2.2440(18) (**12**), 2.252(2) (**13**), 2.2297(15) (**14**), 2.2468(14) (**15**); Pd1–P1 2.3073(18) (**12**), 2.305(2) (**13**), 2.3022 (14) (**14**), 2.2996(17) (**15**); Fe1–Pd1 2.811(3) (**12**), 2.8289(19) (**13**), 2.8184(9) (**14**), 2.8349(11) (**15**); N1–Pd1–P2 159.59(17) (**12**), 158.9(2) (**13**), 158.79(13) (**14**), 160.45(16) (**15**).

N,N ligand scaffolds compared with their P,P counterparts, whereas for related mixed P,N scaffolds, intermediate Pd–Fe distances can be anticipated. In turn that means only Pd–Fe distances for the same ligand scaffold are suitable for meaningful comparison. Remarkably, the Fe–Pd distances observed in complex **10** are the shortest for such ferrocenylene bridged bisphosphane ligands, observed so far. Considering the two independent molecules in the unit cell the Fe–Pd distances in **10** are 2.8369(10) Å and 2.7974(10) Å averaging to 2.817(1) Å, which all are substantially shorter than previously reported values for such complexes, ranging between 2.877(2)–3.0168(4) Å (entries 1–5, Table 1).[85–89] Moreover, the short Fe–Pd contact in **10** comes with $C^{ipso,Cp,Fc}$–P distances (1.790(5) and 1.797(5) Å for Molecule $\mathbf{10^B}$, Table S2, ESI‡) complying to the average values of previously reported complexes (1.783–1.829 Å, entries 1–5, Table 1).[85–89] Similarly complex **11** derived from P,N ligand **3a**, features the shortest Fe–Pd contact for ferrocenylene bridged P,N ligands, observed so far. The Fe–Pd distance in **11** is 2.7384(18), which is shorter than previously reported values for such complexes ranging between 2.7590(5) to 2.7956(5) Å (entries 7 and 8, Table 1).[66,67] By contrast, for the dicationic Pd complexes **12–15** derived from P,N ligand **3a**, the longest Fe–Pd distances are also observed (2.811(3)–2.8349(11) Å, entry 9, Table 1), as compared to the previously reported complexes with ferrocene based P,N ligands (2.7590(5)–2.7956(5) Å, entries 7 and 8, Table 1).[66,67]

The short Fe–Pd distance in complex **10** may be interpreted as an attractive bonding interaction between these two metal centers. However, such a short contact may also be considered as a consequence of a large torsion (τ) or bite angle (β_n) at the structurally flexible ferrocene scaffold owing to steric repulson between substituents R's around Pd (Fig. 6). Comparing the geometric parameters of the complex with the shortest Fe–Pd distance, **10**, with related compounds, all three angular parameters show intermediate values. The tilt angle α (21.5°) in **10** is slightly smaller than that observed with a corresponding dppf complex (22.1°),[86] yet larger than for its Fc′(P^tBu_2)$_2$ analog (16.3°) (entries 1, 3 and 6, Table 1).[89] Bite angle β_n (161.60(5)° and 161.46(5)°) in **10** is slightly smaller than that observed with its Fc′(P^tBu_2)$_2$ analog (162.34(2)°),[85,88] yet larger

Table 1 Molecular parameters of cationic Pd(II) complexes of dppf and its diphospha- and azaphospha-analogs with Fe → Pd bonding interactions[a]

	Square-planar Pd(II) complexes	Avg. $C^{ipso,Cp}$–E bond length[b] (Å)	Pd–Fe distance (Å)	Tilt angle α[c] (°)	Bite angle β_n (°)	Torsion angle τ[c] (°)	Ref.
1	[dppf·Pd(PPh$_3$)][BF$_4$]$_2$	1.787[e] (E = P)	2.8934[e]	19.7[e]	156.79[e]	41.1	85 and 87
	[dppf·PdP(C$_5$H$_4$-*p*-F)$_3$][BF$_4$]$_2$	1.784 (E = P)	3.0014(4)	22.1	157.54(3)	26.9	86
2	[Fc′(P^{t}Bu$_2$)(PPh$_2$)·Pd(PPh$_3$)][BF$_4$]$_2$	1.785(3) (E = P^{tBu}), 1.777(3) (E = P^{Ph})	2.9310(5)	19.7	156.11(3)	42.6	85
3	[Fc′(P^{t}Bu$_2$)$_2$·PdCl][SbCl$_6$]	1.797 (E = P)	2.9389(4)	19.8	162.34(2)	30.5	85
	[Fc′(P^{t}Bu$_2$)$_2$·PdI][I]	1.823[e] (E = P)	2.9390[e]	18.0[e]	161.88[e]	34.6	85 and 88
	[Fc′(P^{t}Bu$_2$)$_2$·PdBr][TFAB][d]	1.829 (E = P)	2.9395(18)	19.2	163.04(5)	31.0	88
	[Fc′(P^{t}Bu$_2$)$_2$·Pd(C$_6$H$_4$-*p*-CN)][BF$_4$]$_2$	1.808 (E = P)	2.9988(8)	16.3	159.75(4)	35.9	89
4	[Fc′[P(C$_6$H$_{11}$)$_2$]$_2$·Pd(PPh$_3$)][BF$_4$]$_2$	1.782 (E = P)	2.9339(5)	18.9	156.63(3)	38.2	85
	[Fc′[P(C$_6$H$_{11}$)$_2$]$_2$·Pd(PMe$_3$)][BF$_4$]$_2$	1.783 (E = P)	2.9567(10)	20.4	157.20(6)	41.7	85
5	[Fc′(CpP^{i}Pr$_2$)$_2$·Pd(PMe$_3$)][BF$_4$]$_2$	1.786 (E = P)	3.0168(4)	19.1	158.09(2)	32.6	85
6	[Fc′(PMes$_2$)(P^{t}Bu$_2$)·PdCl][SbF$_6$] (**10**)[e]	1.795 (E = P^{tBu})[e] and 1.788 (E = P^{Mes})[e]	2.8369(10) and 2.7974(10)	21.5[e]	161.60(5)° and 161.46(5)°	40.5 and 46.2	h
7	[Fc′[NC(NH^{i}Pr)$_2$](PPh$_2$)·PdCl][SbF$_6$]	1.775(2) (E = P) and 1.379(3) (E = N)	2.7590(5)	24.6	163.01(5)	1.9	66
	[Fc′[NC(NHCy)$_2$](PPh$_2$)·PdCl][SbF$_6$][f]	1.773(2) (E = P) and 1.388(2) (E = N)	2.7956(5)	22.8	162.46(5)	5.7	66
	[Fc′[NC(NHXyl)$_2$](PPh$_2$)·PdCl][SbF$_6$][g]	1.770(2) (E = P) and 1.384(2) (E = N)	2.7821(5)	23.0	163.15(5)	5.9	66
8	[Fc′[NH(CH$_2$)$_2$PPh$_2$](PPh$_2$)·Pd][SbF$_6$]$_2$	1.790(7) (E = P) and 1.419(9) (E = N)	2.7889(9)	21.3	164.4(2)	9.8	67
9	[Fc′(PPh$_2$)(NMe$_2$)·PdCl][SbF$_6$]$_2$ (**11**)	1.783(11) (E = P) and 1.394(15) (E = N)	2.7384(18)	23.3	163.9(2)	1.7	h
	[Fc′(PPh$_2$)(NMe$_2$)·Pd(PPh$_2$C$_5$H$_5$)][SbF$_6$]$_2$ (**12**)	1.788(8) (E = P) and 1.420(9) (E = N)	2.811(3)	21.9	159.11(19)	22.3	h
	[Fc′(PPh$_2$)(NMe$_2$)·Pd(PPh$_3$)][BF$_4$]$_2$ (**13**)	1.758(10) (E = P) and 1.415(12) (E = N)	2.8289(19)	20.9	158.9(2)	20.4	h
	[Fc′(PPh$_2$)(NMe$_2$)·Pd(PPh$_2$)Fc′(NMe$_2$)][BF$_4$]$_2$ (**14**)	1.766(6) (E = P) and 1.427(7) (E = N)	2.8184(9)	19.5	158.79(13)	30.7	h
	[Fc′(PPh$_2$)(NMe$_2$)·PdP(*p*-OMe-C$_6$H$_4$)$_3$][BF$_4$]$_2$ (**15**)	1.770(7) (E = P) and 1.408(9) (E = N)	2.8349(11)	22.5	160.45(16)	11.1	h

[a] Entire table is available in ESI, Table S1.‡ [b] Averages of two identical bonds from a single molecule (standard deviations are excluded). [c] Angles were calculated using Mercury as crystallographic software.[90,91] [d] TFAB = tetrakis(pentafluorophenyl)borate,[88] $[B(C_6F_5)_4]^-$. [e] Averages from all crystallographically independent entities in the unit cell (standard deviations are excluded). [f] Cy = C_6H_{11}. [g] Xyl = 2,4,6-Me$_3$-C$_6$H$_2$. [h] Presented in current report.

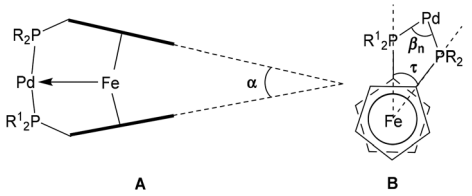

Fig. 6 Molecular parameters of Pd(II) complexes of dppf analogs with Fe → Pd interactions with bite (β_n), torsion (τ), and tilt (α) angles illustrated.

than for its Fc′(P^{t}Bu$_2$)(PPh$_2$)·analog (156.11(3)°) (entries 1, 3 and 6, Table 1).[85]

While the torsion angle for **10** is 40.5°, the largest and smallest τ-values in related complexes are found for its Fc′(P^{t}Bu$_2$)(PPh$_2$)·analog (42.6°)[85] and its dppf analog (26.9°),[86] respectively (entries 1, 2 and 6, Table 1). In summary, these values indicate that the Fe–Pd distance is not a consequence of either steric repulsion or geometric distortion alone in the related molecule. In turn, the unusual shortening of Fe–Pd bond in compound **10** seems to be a compromise between minimized steric repulsion, rotational distortion, and secondary interaction of the ligand system in the solid state. Similarly, **11**, featuring the shortest Fe–Pd bond reported for this complex type involving a P,N ligand shows no unusual bite (β_n = 163.9(2)°) torsion (τ = 1.7°) and tilt (α = 23.3°) angles compared with previously reported analogs (entries 7–9, Table 1).[66,67]

For complexes **11–15** derived from P,N ligand **3a**, the longest Fe–Pd distances had been observed. Interestingly, the torsion angles in **12–14** are 22.3° (**12**), 20.4° (**13**) and 30.7° (**14**) the largest found so far, where for related complexes values between 1.9–9.8° had been reported (entries 7–9, Table 1).[66,67] Compared to its Fc′(NMe$_2$)(PPh$_2$) congeners **12–14** the torsion angle of **15** is slightly smaller (11.1°). Regarding their bite angles β_n, complexes **11–15** feature lower values (158.79(13)°–163.9(2)°) as compared to previously reported related structures (162.46(5)–164.4(2)°) (entries 7–9, Table 1).[66,67] Similarly, the tilt angles in complexes **11–15** are between 19.5° and 23.3°, slightly smaller compared to those for related complexes Fc′[NC(NHR)$_2$](PPh$_2$)·[PdCl][SbF$_6$] (R = ^{i}Pr, Cy and Xyl; entry 7,

Table 1) and Fc′[NH(CH$_2$)$_2$PPh$_2$][PPh$_2$]·Pd[SbF$_6$]$_2$ (entry 8, Table 1) reported so far (21.3°–24.6°).[66,67]

To get deeper insight into the proposed interaction between the iron and palladium centers, DFT calculations were carried out (more details in the ESI‡). First, different DFT methods were tested on systems **10–15** (see Table S19, ESI‡) and the optimized geometries were compared with the obtained X-ray structures. Although the computed and X-ray structures are in good agreement, as a common motif the differences between the DFT calculated and the experimentally obtained Fe–Pd distances vary between 0.059–0.212 Å (Table S19, ESI‡). Without any doubt, it can be considered as a noticeably high error, especially if the description of the interaction between these two atoms is the main goal. One possible explanation of such discrepancy could be a flat potential energy surface (PES). Therefore, to test the plausibility of our inference, we performed PES scans with incremental increase or decrease of the Fe–Pd distances.[92] First, three model systems were computed, where the bulky groups were repleaced by methyl substituents (**16–18**, Fig. 7) in order to keep the steric factors less dominant. Similar to our previuos study,[93] the best match between computed and experimental structures was obtained using the ωB97X-D funcional, which was then employed for optimizing the molecular structures in this study. It can further be established that all the three structures are very flexible, where 0.200 Å elongation or contraction require only 1.0–4.8 kcal mol^{-1} energy investment and the flexibility increases in the order of **18** > **17** > **16**. In case of **18**, 0.3 Å stretching requires energy as low as 2.5–3.6 kcal mol^{-1}. These data suggest a rather weak interaction between the two metals, especially in case of **18**. In full agreement with our present study, only 2.3 kcal mol^{-1} stabilization energy was reported for [Pd(dtbpf)Cl]$^+$.[85] Such small energy values can easily be compensated by second order interactions in the crystal lattice.

This hypothesis was fully supported by the X-ray structure of **10** where two independent molecules are present in the crystallographic unit cell differing in their geometric parameters, but otherwise feature identical steric and electronic parameters based on their identical constitution. However, careful comparison pointed at two separate, yet apparently interconnected, differences between them. When one molecule has a torsion angle substantially higher (46.2°) than the other (40.5°), the latter shows comparatively higher Pd–Fe distance (2.8369(10) Å) than the earlier (2.7974(10) Å) (Table S2, ESI‡). However, such correlation between molecular torsion and Pd–Fe distance is not completely uncommon in the literature and can further be observed for similar dppf-complexes depicted in Table 1 (entry 1), where [dppf·PdP(C$_5$H$_4$-*p*-F)$_3$][BF$_4$]$_2$ shows higher Pd–Fe distance but lower torsion angle than [dppf·Pd(PPh$_3$)][BF$_4$]$_2$. The remaining molecular parameters for aforementioned independent molecular entities of **10** are quite comparable, and sometimes equal in magnitude once the standard deviations are carefully considered (Table S1, ESI‡).

In case of the related compound [Fc′(NIm)$_2$·Pd(NCMe)]$^{2+}$, Tamm and co-workers demonstrated that the possible existence of a second (local) minimum on the PES, where the Fe–Pd distance is significantly longer.[92] Therefore, we have further increased the distance between Pd and Fe centers in case of the model systems (**16–18**) and second minima were found around ~3.78 Å (**16′**), ~4.01 Å (**17′**) and ~4.29 Å (**18′**), and the Pd atom adopts a slightly distorted T-shaped geometry, which is in full agreement with the earlier knowledge.[92] In contrast to **16** and **17**, in case of **18** the T-shaped, second minima (**16′**, **17′**, **18′**) is more stable by 8.1 kcal mol^{-1} ($\Delta E_{\text{isomer-scan}}$, Fig. 7).

Starting a new optimization without any restriction from the T-shaped structure (**18′**) verified the stability of this second isomer at higher level of theory as well (ΔE_{isomer} = −8.8 kcal mol^{-1} at ωB97X-D/6-311+G**), which further suggests a rather weak Fe–Pd interaction for **18**. A similar conclusion can be obtained performing the same calculations with the dppf ligand (ΔE_{isomer} = −9.4 kcal mol^{-1} at ωB97X-D/6-311+G**). As expected, on further increasing steric hindrance the energy difference between the two isomers decreases and the stability order changes at a certain point.

Indeed, performing PES scans on compounds **10** and **18** revealed that the T-shaped isomers become more stable by 12.5 kcal mol^{-1} in case of **10**. In contrast to **10**, compound **11** (with rather less bulky substituents at the donor atoms) did not significantly differ from the model compound **17**, *i.e.* the T-shaped isomer is less stable for **11** ($\Delta E_{\text{isomer-scan}}$ = 11.9 kcal mol^{-1} for **11** and $\Delta E_{\text{isomer-scan}}$ = 8.8 kcal mol^{-1} for **17**, Fig. 7 and 8). Nataro and co-workers came to a similar conclusion, where introduction of two bulky *tert*-butyl groups at both phosphorus atoms (*i.e.* for d*t*bpf ligand) was able to prevent the formation of the T-shaped isomer, which in turn further prevented dimerization *via* formation of intermolecular Pd$_2$Cl$_2$ bridging unit (Fig. S62, ESI‡).[85] Similarly, once the chlorine substituent was replaced by the more bulky phosphane ligands (**12–15**), the stability of the molecule with T-shaped geometry at Pd centres substantially decreased due to steric factors (compare PES scan for **17** and **12–15** in Fig. 7 and 8).

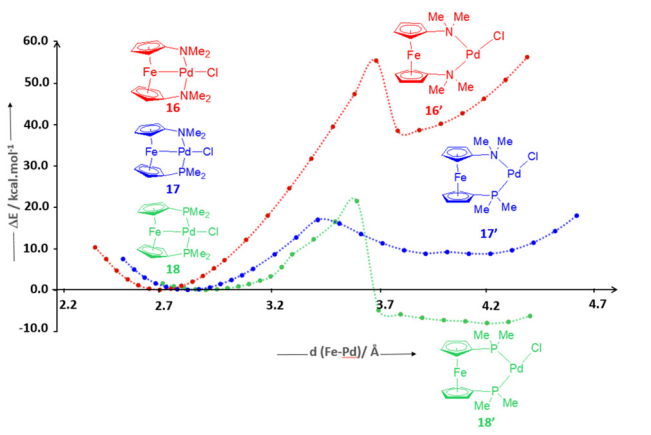

Fig. 7 Potential energy surface (PES) scan for the elongation of the Fe–Pd distance in the model compounds **16–18**.

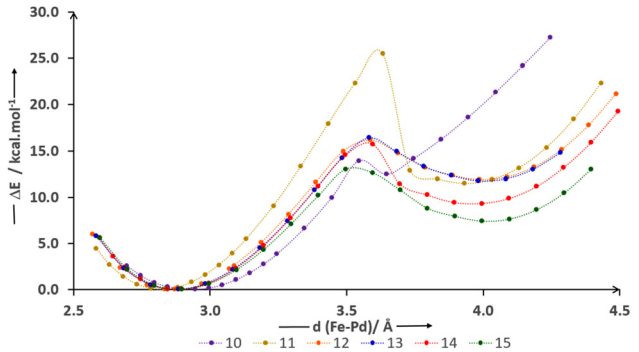

Fig. 8 Potential energy surface (PES) scan for the elongation of the Fe–Pd distance for the compounds **10–15**.

Apart from investigation of the energetic aspects, Kohn–Sham molecular orbitals of **10–15** (Fig S63 in the ESI‡) and Wiberg-indices of the Fe–Pd bonds, and Bader's Atoms-in-molecules (AIM) topology analyses (Tables S20, S21–S23 in the ESI‡) were performed in case of all investigated points of the PES scans of **16–18**. Unsurprisingly, both descriptors suggest a stronger bond between the metal centers if the actual Fe–Pd distance is shorter. Interestingly, both the bond critical points and the Wiberg-indices exhibit almost perfect linear trends with the Fe–Pd bond lengths. Since the different DFT functionals deliver various Pd–Fe distances, the use of these descriptors requires careful application and serious consideration.

In line with the presence of a Fe → Pd bond, variation of a competing donor affects the Fe–Pd bond length. As compared to compounds **11–14**, compound **15** contains a higher electron donating phosphine P(*p*-OMe-C_6H_4)$_3$, and consequently an electronically more saturated Pd(II) atom.[86] As a result, compound **15** shows a weaker and consequently longer Pd–Fe bond [2.8349(11) Å], as compared to those of **11** (2.7384(18) Å), **12** (2.811(3) Å), **13** (2.815(2) Å) and **14** (2.8184(9) Å) (entry 9, Table 1). The calculated bond lengths exhibit similar trends.

CV measurements have been made to explore how the redox properties of the ferrocene unit change through the interaction with the Pd(II) atom. While $PdCl_2$ complex **8** shows a quasi-reversible oxidation with a half wave potential of 0.15 V (Fig. S1, ESI‡), upon chloride abstraction no comparable oxidation event was detectable for its cationic analog **10**. For the related P,N complexes **11**, **13** and **15** also no structured oxidation events were found. Only **14** shows a broad irreversible oxidation with a maximum at 1.10 V (Fig. S1, ESI‡), which we attribute to the P-coordinated freely rotating ferrocene moiety with an uncoordinated NMe_2 unit only present in this compound. For the reduction of the complexes **13–15** on the other hand irreversible maxima were detected at −0.85 V (**13**), −1.20 V (**14**) and −0.89 V (**15**) (Fig. S1, ESI‡). These results suggest that Fe → Pd interactions are fairly strong in these complexes and consequently the Fe atom is no longer available for reversible oxidation within the potential window of the solvent.

General experimental section

All manipulations were performed under argon atmosphere unless mentioned otherwise. Prior to use, the glassware was dried in a drying oven at 120 °C. Solvents were distilled over drying agents, prescribed in the CRC Handbook of chemistry and subsequently stored under argon atmosphere over 4 Å molecular sieves. Solvents for column chromatography and aqueous workups were used (analytical grade supplied by VWR and Alfa-Aesar) without further purification. NMR solvents (purchased from Deutero) were degassed *via* a few cycles of freeze, pump and thaw, and finally stored over 3 Å molecular sieves under Argon atmosphere. Reagents and chemicals were purchased from commercial suppliers (Sigma-Aldrich, ABCR, Alfa-Aesar) and used as received. Ligands Fc′($PMes_2$)(PPh_2)[83] and Fc′($PMes_2$)(P^tBu_2)[82] were synthesized following procedures, reported by Pietschnig *et al.*[94] Although Fc′(NH_2)Br has previously been synthesized following various procedures in yields of 71%,[74] and 50% (calculated on the basis of starting Fc′Br_2),[73,77] in the current report, a recently published procedure was employed, due to its simplicity and higher yield (*ca.* 70–80%, calculated on the basis of Fc′Br_2).[78]

All solution-phase NMR spectra were measured with Varian 500VNMRS and Varian MR-400 spectrometers at 22 °C. Chemical shifts (δ in ppm) were expressed with respect to the following standards, set as 0 ppm: $SiMe_4$ (for ^{1}H and ^{13}C), aqueous H_3PO_4 (for ^{31}P), $BF_3{\cdot}OEt_2$ (in $CDCl_3$ for ^{11}B) and $CFCl_3$ (for ^{19}F). The signals, resulting from the residual non-deuterated NMR solvents, were referenced as indicated in the literature.[95] In addition to the standard notation of the signal multiplicity, pst, brs, brd and brm were used to abbreviate pseudo triplet, broad singlet, broad doublet and broad multiplet, respectively in order. The amount of residual solvents was verified by NMR analysis and the expected values for elemental analyses were calculated accordingly. When Electrospray ionization (ESI) and Atmospheric pressure chemical ionization (APCI) mass spectra were measured with a Finnigan LCQ Deca (ThermoQuest, San Jose, USA) instrument using samples dissolved in HPLC-quality thf, MALDI was measured with an UltraFlex ToF/ToF (Bruker Daltonics, Bremen, D) instrument, where an N_2 laser with 337 nm wavelength and 3 ns pulse duration was used. Elemental analyses were performed without the presence of any external oxidizer in an EA 3000 Elemental Analyzer (EuroVector). The values of elemental analyses, reported in this article is actually the average of three consecutive readings taken from the purest specimens of each compound. X-ray diffraction experiments were performed using a STOE StadiVari [using either Mo-GENIX source (λ = 0.71073 Å), or Cu-GENIX source (λ = 1.54186 Å)] diffractometer. Structures were solved using dual space method (SHELXT) and were refined with SHELXL-2018.[96] All non-hydrogen atoms were refined anisotropically, whereas hydrogen atoms were placed on adjacent atoms using a riding model. Further programs used in the structure analyses were Mercury and Platon.[97–99]

CV measurement was done with GB2202-C-VAC under Argon atmosphere, when samples were measured as a solution

(1 mM) in dry and deoxygenated CH_2Cl_2, where anhydrous $[Bu_4N][PF_6]$ was used as a conducting salt at a concentration of 0.1 M. The three-electrode cell consisted of a platinum working electrode, a silver counter electrode, and a silver pseudo reference electrode. The potential was driven on a WaveDriver 20 Bipotentiostat from Pine Research Instrument, and the electrochemical data was recorded *via* AfterMath (Ver. 1.5.9807, Pine Instrument). All redox processes were referenced using half-wave potentials of $Fe(C_5Me_5)_2$ as a standard, which was added to the analysed solution. Its corresponding value was then subtracted from the recorded potentials to convert them to the Fc/Fc^+ scale following established procedures,[100] and finally evaluated with AfterMath and OriginPro.

Fc′(NMe$_2$)Br (2)

On the basis of a known procedure to synthesize Fc′($NHCH_2R$)Br (when R = Ph, ^{t}Bu),[77] A solution of Fc′(NH_2)Br (0.660 g, 2.36 mmol) in glacial acetic acid (18 mL) under argon was treated with paraformaldehyde (0.707 g, 23.54 mmol) and $NaBH_3CN$ (0.740 g, 11.78 mmol) and stirred at room temperature overnight. The reaction mixture was brought to pH 12 by addition of 60 mL of 10 M aqueous solution of NaOH and extracted with hexanes (4 × 20 mL). The combined organic extract was washed with water and brine, dried over anhydrous Na_2SO_4 and filtered. Column chromatography was performed on SiO_2, using a solution of hexanes and NEt_3 (98 : 2). After removal of volatiles in high vacuum, compound Fc′(NMe_2)Br was recovered as dark red oil (0.659 g, 2.14 mmol, 91%), which is slightly sensitive towards aerial oxygen and solidifies over standing for long time at rt. ^{1}H NMR (C_6D_6): δ 2.27 (s, 6H, –NCH_3), 3.54 (pst, 2H, α-H of $C_5H_4^{NMe2}$), 3.86 (pst, 2H, α-H of $C_5H_4^{Br}$), 3.89 (pst, 2H, β-H of $C_5H_4^{NMe2}$), 4.42 (pst, 2H, β-H of $C_5H_4^{Br}$). ^{13}C NMR (C_6D_6): δ 41.95 (s, –NCH_3), 57.66 (s, C of $C_5H_4^{NMe2}$), 66.17 (s, C of $C_5H_4^{NMe2}$), 66.42 (s, C of $C_5H_4^{Br}$), 69.09 (s, C of $C_5H_4^{Br}$), 78.54 (s, *ipso*-C of $C_5H_4^{Br}$). MS (APCI) 308 [M], 309 [M + 1]. Anal. Calcd for $C_{12}H_{14}BrFeN$: C, 46.80; H, 4.58; N, 4.55. Found C, 46.69; H, 4.66; N, 4.63.

Fc′(NMe$_2$)(PPh$_2$) (3a)

^{n}BuLi (0.9 mL, 2.5 M in hexanes, 2.25 mmol) was added dropwise to a 0 °C cooled solution of Fc′(NMe_2)Br (0.659 g, 2.14 mmol) in a mixture of hexanes and thf (30 mL; hexanes : thf; 9 : 1), resulting in a color change from pale yellow to bright orange. After the reaction mixture was stirred for 40 min at 0 °C, a solution of Ph_2PCl (2.40 mmol) in a mixture of hexanes and thf (30 mL; hexanes : thf; 9 : 1) was added dropwise over *ca.* 5 minutes. The reaction mixture was warmed to ambient temperature and stirred overnight. After all the volatiles were removed under high vacuum, the product was extracted in a mixture of hexanes and toluene (50 mL, hexanes : toluene, 2 : 1), and LiCl was removed by filtration. From this orange solution, solvents were removed under high vacuum, resulting in a yellow, sticky solid, which was further purified by crystallization in a mixture of hexanes and toluene (10 mL, hexanes : toluene, 4 : 1) at −20 °C (crystallized yield 76%). ^{1}H NMR (Toluene D8): δ 2.21 (s, 6H, –NCH_3), 3.54 (pst, 2H, α-H of $C_5H_4^{NMe2}$), 3.74 (pst, 2H, α-H of $C_5H_4^{PPh2}$), 4.20 (pst, 2H, β-H of $C_5H_4^{NMe2}$), 4.33 (pst, 2H, β-H of $C_5H_4^{PPh2}$), 7.04–7.09 (m, 6H, *m*-, *p*-H^{Ph}), 7.44–7.48 (m, 4H, *o*-H^{Ph}). ^{13}C NMR (Toluene D8): δ 41.87 (s, –NCH_3), 56.16 (s, C of $C_5H_4^{NMe2}$), 65.10 (s, C of $C_5H_4^{NMe2}$), 69.77 (d, β-C of $C_5H_4^{PPh2}$, J = 4 Hz), 72.21 (d, α-C of $C_5H_4^{PPh2}$, J = 15 Hz), 75.41 (d, *ipso*-C of $C_5H_4^{PPh2}$, J = 7 Hz), 116.64 (s, *ipso*-C of $C_5H_4^{NMe2}$), 128.38 (d, *m*-C^{Ph}, J = 9 Hz), 134.00 (d, *o*-C^{Ph}, J = 20 Hz), 140.69 (d, *p*-C^{Ph}, J = 12 Hz). ^{31}P{^{1}H} NMR (Toluene D8): δ −16.1 (s, *P*Ph_2). MS (APCI) 414 [M + 1]. Anal. Calcd for $C_{24}H_{24}FeNP$: C, 69.75; H, 5.85; N, 3.39. Found: C, 69.88; H, 5.97; N, 3.31.

Fc′(NMe$_2$)(PMes$_2$) (3b)

^{n}BuLi (0.9 mL, 2.25 mmol) was added dropwise to a 0 °C cooled solution of Fc′(NMe_2)Br (0.659 g, 2.14 mmol) in a mixture of hexanes and thf (30 mL; hexanes : thf; 9 : 1), resulting in a color change from pale yellow to bright orange. After the reaction mixture was stirred for 40 min at 0 °C, a solution of Mes_2PX (X = Cl/Br, 48%/52%, FW = 327.914 g mol^{-1}, 2.50 mmol) in a mixture of hexanes and thf (30 mL; hexanes : thf; 9 : 1) was added dropwise over *ca.* 5 minutes. The reaction mixture was warmed to ambient temperature and stirred overnight. After all the volatiles were removed under high vacuum, the product was extracted in a mixture of hexanes and toluene (50 mL, hexanes : toluene, 2 : 1), and LiCl was removed by filtration. From this orange solution, solvents were removed under high vacuum, resulting in a yellow, sticky solid, which was further purified by crystallization in a mixture of hexanes and toluene (10 mL, hexanes : toluene, 4 : 1) at −20 °C. Crystallized yield 23%. ^{1}H NMR (Toluene D8): δ 2.09 (m, 6H, *p*-CH_3 of Mes), 2.11 (m, 12H, *o*-CH_3 of Mes), 2.38 (bs, 6H, –NCH_3), 3.52 (m, 2H, α-H of $C_5H_4^{NMe2}$), 3.84 (m, 2H, α-H of $C_5H_4^{PMes2}$), 4.34 (m, 2H, β-H of $C_5H_4^{NMe2}$), 4.45 (m, 2H, β-H of $C_5H_4^{PMes2}$), 6.69 (brs, 4H, *m*-H^{Mes}). ^{13}C NMR (Toluene D8): δ 20.84 (s, *p*-CH_3^{Mes}), 23.52 (d, *o*-CH_3^{Mes}, J = 15 Hz), 41.53 (s, –NCH_3), 56.14 (s, C of $C_5H_4^{NMe2}$), 65.00 (s, C of $C_5H_4^{NMe2}$), 69.46 (d, β-C of $C_5H_4^{PPh2}$, J = 4 Hz), 74.27 (d, α-C of $C_5H_4^{PPh2}$, J = 19 Hz), 77.49 (d, *ipso*-C of $C_5H_4^{PPh2}$, J = 11 Hz), 116.56 (s, *ipso*-C of $C_5H_4^{NMe2}$), 130.41 (d, *m*-C^{Ph}, J = 3 Hz), 133.41 (d, *o*-H^{Ph}, J = 21 Hz), 142.50 (d, *p*-H^{Ph}, J = 15 Hz). ^{31}P{^{1}H} NMR (Toluene D8): δ −33.9 (s, *P*Mes_2). MS (APCI): *m*/*z* (%) 498 [M + 1]. HRMS (APCI) 498.2008 [M + 1]. Anal. Calcd for $C_{30}H_{36}FeNP$: C, 72.44; H, 7.29; N, 2.82. Found: C, 72.56; H, 7.36; N, 2.88.

Selenophosphoranes of Fc′(NMe$_2$)(PPh$_2$) (3a) and Fc′(NMe$_2$)(PMes$_2$) (3b)

On the basis of a known procedure,[82,83] a suspension of red Se (0.5 mmol) and Fc′(NMe_2)(PPh_2) or Fc′(NMe_2)($PMes_2$) (0.2 mmol) in thf (20 mL) was stirred for 1 h at r.t. All the volatiles were removed under high vacuum (10^{-3} mbar) and the product was extracted with hot toluene. Analytically pure compound was precipitated from hot toluene by slow cooling. *Note*: If all the residual Se is not removed by single filtration attempt, the procedure of filtration must be carried out for multiple times before characterization.

Fc′(NMe$_2$)(PSePh$_2$) (4a)

Yield 86%. ^{1}H NMR (Toluene D8): δ 2.09 (s, 6H, –NCH_3), 3.63 (pst, 2H, α-H of $C_5H_4^{NMe2}$), 3.90 (pst, 2H, β-H of $C_5H_4^{NMe2}$), 4.38 (m, 2H, α-H of $C_5H_4^{PSePh2}$), 4.56 (m, 2H, β-H of $C_5H_4^{PSePh2}$), 6.95–7.00 (m, 6H, *m*-, *p*-H^{Ph}), 7.80–7.85 (m, 6H, *o*-H^{Ph}). ^{13}C NMR (Toluene D8): δ 41.67 (s, –NCH_3), 56.56 (s, C of $C_5H_4^{NMe2}$), 66.56 (s, C of $C_5H_4^{NMe2}$), 70.61 (d, β-C of $C_5H_4^{PSePh2}$, J = 10 Hz), 72.84 (d, α-C of $C_5H_4^{PSePh2}$, J = 15 Hz), 117.63 (s, *ipso*-C of $C_5H_4^{NMe2}$), 128.08 (d, *o*-C^{Ph}, J = 12 Hz), 130.81 (d, *m*-C^{Ph}, J = 3 Hz), 132.55 (d, *p*-C^{Ph}, J = 11 Hz), 135.30 (d, *ipso*-C of Ph). ^{31}P{^{1}H} NMR (Toluene D8): δ 36.7 (s, *P*SePh$_2$, $^1J_{P–Se}$ = 757 Hz). ^{77}Se NMR (toluene-d8): δ −296.3 (d, P*Se*Ph$_2$, $^1J_{P–Se}$ = 757 Hz). MS (MALDI) 493 [M]. Anal. Calcd for $C_{24}H_{24}$SeFeNP: C, 58.56; H, 4.91; N, 2.85. Found: C, 58.83; H, 4.96; N, 2.90.

Fc′(NMe$_2$)(PSeMes$_2$) (4b)

Yield 93%. ^{1}H NMR (Toluene D8): δ 1.99 (s, 6H, *p*-CH_3 of Mes), 2.17 (s, 6H, –NCH_3), 2.47 (bs, 12H, *o*-CH_3 of Mes), 3.66 (bs, 2H, β-H of $C_5H_4^{PSeMes2}$), 4.03 (m, 2H, α-H of $C_5H_4^{NMe2}$), 4.42 (m, 2H, β-H of $C_5H_4^{NMe2}$), 5.01 (bs, 2H, α-H of $C_5H_4^{PSeMes2}$), 6.54 (bd, 4H, *m*-H of Mes, J = 4 Hz). ^{13}C NMR (Toluene D8): δ 24.47 (d, *C*H$_3$ of Mes, J = 6 Hz), 41.55 (s, –N*C*H$_3$), 56.89 (s, β-C of $C_5H_4^{NMe2}$), 66.81 (s, α-C of $C_5H_4^{NMe2}$), 70.58 (d, β-C of $C_5H_4^{PSeMes2}$, J = 10 Hz), 76.08 (d, *ipso*-C of $C_5H_4^{PSeMes2}$, J = 10 Hz), 79.14 (d, α-C of $C_5H_4^{PSeMes2}$, J = 81.0 Hz), 117.54 (s, *ipso*-C of $C_5H_4^{NMe2}$), 131.90 (d, *o*-C^{Ph}, J = 11 Hz), 139.28 (d, *m*-C^{Ph}, J = 3 Hz), 140.51 (bs, *ipso*-C^{Ph}). ^{31}P{^{1}H} NMR (Toluene D8): δ 15.8 (s, *P*SeMes$_2$, $^1J_{P–Se}$ = 719 Hz). ^{77}Se NMR (Toluene D8): δ −79.5 (d, P*Se*Mes$_2$, $^1J_{P–Se}$ = 719 Hz). MS (MALDI) 578 [M + 1]. Anal. Calcd for $C_{30}H_{36}$SeFeNP: C, 62.51; H, 6.30; N, 2.43. Found: C, 62.69; H, 6.55; N, 2.48.

PdCl$_2$ Complexes of Fc′(PMes$_2$)(PPh$_2$) (5), Fc′(PMes$_2$)(P^{t}Bu$_2$) (6) and Fc′(NMe$_2$)(PPh$_2$) (3a)

On the basis of a known procedure,[33,54,101] a suspension of PdCl$_2$ (0.1 mmol) and Fc′(PMes$_2$)(PPh$_2$) (**5**, 0.1 mmol) or Fc′(PMes$_2$)(P^{t}Bu$_2$) (**6**, 0.1 mmol) or Fc′(NMe$_2$)(PPh$_2$) (**3a**, 0.2 mmol) in DCM (20 mL) was stirred for 1 h at r.t. Analytically pure crystalline materials were obtained from DCM solution by slow diffusion of dry pentane at room temperature.

Fc′(PMes$_2$)(PPh$_2$)·PdCl$_2$ (7)

Yield 81%. ^{1}H NMR (CD_2Cl_2): δ 1.64 (s, 3H, CH_3 of Mes), 1.86 (s, 3H, CH_3 of Mes), 2.23 (s, 3H, CH_3 of Mes), 2.29 (s, 3H, CH_3 of Mes), 2.61 (s, 3H, CH_3 of Mes), 3.32 (s, 3H, CH_3 of Mes), 3.58 (bs, 1H, H of C_5H_4), 4.14 (bs, 1H, H of C_5H_4), 4.15 (bs, 1H, H of C_5H_4), 4.20 (bs, 1H, H of C_5H_4), 4.37 (bs, 2H, H of C_5H_4), 4.56 (bs, 1H, H of C_5H_4), 5.59 (bs, 1H, H of C_5H_4), 6.67 (m, 1H, *m*-H of Mes), 6.79 (m, 1H, *m*-H of Mes), 6.84 (m, 1H, *m*-H of Mes), 6.90 (m, 1H, *m*-H of Mes), 7.44–7.57 (bm, 6H, *m* and *p*-H of Ph), 7.89–7.93 (bm, 2H, *o*-H of Ph), 8.09–8.13 (bm, 2H, *o*-H of Ph). ^{13}C NMR (CD_2Cl_2): δ (126 MHz, CD_2Cl_2) δ 20.94 (d, *C*H$_3^{Mes}$, J = 9 Hz), 25.38 (d, *C*H$_3^{Mes}$, J = 7 Hz), 25.85 (d, *C*H$_3^{Mes}$, J = 2.4 Hz), 27.63 (d, *C*H$_3^{Mes}$, J = 7 Hz), 28.50 (dd, *C*H$_3^{Mes}$, J = 15, 5 Hz), 71.74 (d, H of C_5H_4, J = 6 Hz), 72.40 (d, H of C_5H_4, J = 5 Hz), 74.52 (d, H of C_5H_4, J = 10 Hz), 74.73 (d, H of C_5H_4, J = 7 Hz), 74.94 (d, H of C_5H_4, J = 12 Hz), 76.28 (dd, *ipso*-H of C_5H_4, J = 52, 6 Hz), 78.29 (d, H of C_5H_4, J = 6 Hz), 78.40 (d, H of C_5H_4, J = 4 Hz), 80.34 (dd, *ipso*-H of C_5H_4, J = 50, 7 Hz), 84.80 (d, H of C_5H_4, J = 22 Hz), 128.45 (dd, *aryl*-H, J = 76, 11 Hz), 130.55–131.03 (m, *aryl*-H), 131.53 (d, *aryl*-H, J = 3 Hz), 132.00 (d, *aryl*-H, J = 7 Hz), 133.25 (dd, *aryl*-H, J = 57, 5 Hz), 135.25 (dd, *aryl*-H, J = 32, 10 Hz), 139.56 (d, *aryl*-H, J = 3 Hz), 139.89 (d, *aryl*-H, J = 8 Hz), 141.53 (d, *aryl*-H, J = 2 Hz), 142.99 (d, *aryl*-H, J = 9 Hz). ^{31}P{^{1}H} NMR (CD_2Cl_2): δ 15.0 (d, *P*Mes, J = 30 Hz), 31.4 (d, *P*Ph, J = 30 Hz). MS (ESI) 780 [M] for $[C_{40}H_{40}FeP_2PdCl]^+$. Anal. calcd for $C_{40}H_{40}Cl_2FeP_2Pd$: C, 58.89; H, 4.94. Found: C, 59.23; H, 5.16.

Fc′(PMes$_2$)(P^{t}Bu$_2$)·PdCl$_2$ (8)

Yield 63%. ^{1}H NMR (CD_2Cl_2): δ 1.25 (s, 3H, CH_3 of Mes), 1.77 (s, 3H, CH_3 of Mes), 1.60–2.10 (bs, 18H, PC(CH_3)$_3$), 2.27 (s, 3H, CH_3 of Mes), 2.27 (s, 3H, CH_3 of Mes), 3.86 (s, 3H, CH_3 of Mes), 3.93 (pst, 1H, H of C_5H_4), 3.96 (s, 3H, CH_3 of Mes), 4.14 (s, 1H, H of C_5H_4), 4.21 (pst, 1H, H of C_5H_4), 4.27 (s, 1H, H of C_5H_4), 4.56 (m, 1H, H of C_5H_4), 4.64 (d, 1H, H of C_5H_4), 4.71 (pst, 1H, H of C_5H_4), 4.94 (m, 1H, H of C_5H_4), 6.66 (m, 1H, *m*-H of Mes), 6.69 (s, 1H, *m*-H of Mes), 6.99 (m, 1H, *m*-H of Mes), 7.05 (m, 1H, *m*-H of Mes). ^{31}P {^{1}H} NMR (CD_2Cl_2): δ 15.8 (d, *P*Mes, J = 34 Hz), 77.3 (d, *P*^{t}Bu, J = 34 Hz). MS (ESI) 740 [M] for cation $[C_{36}H_{48}ClFeP_2Pd]^+$. HRMS (MALDI) 739.1327 $[C_{36}H_{48}FeP_2PdCl]^+$. Anal. calcd for $C_{36}H_{48}Cl_2FeP_2Pd$: C, 55.73; H, 6.24. Found: C, 55.71; H, 5.88. *Note*: Although this compound was synthesized and crystallized from a solution of DCM, the crystallized species is difficult to dissolve in CD_2Cl_2, resulting in precipitation of crystallized compound in the NMR tube during measurement for prolonged time. As a result, the quality of ^{13}C NMR obtained was very poor in terms of signal shape and ratio with base line (Fig. S61‡).

[Fc′(NMe$_2$)(PPh$_2$)]$_2$·PdCl$_2$ (9)

Yield 48%. ^{1}H NMR (Toluene-d_8): δ 2.20 (brm, 12H, NCH_3), 3.48 (brs, 4H, H of C_5H_4), 3.68 (brs, 4H, H of C_5H_4), 4.17 (brs, 4H, H of C_5H_4), 4.39 (brs, 4H, H of C_5H_4), 7.10 (brm, 12H, *aryl*-H), 7.42 (brm, 8H, *aryl*-H). ^{13}C NMR (Toluene-d_8) δ 41.81 (brs, N*C*H$_3$), 56.16 (brs, C of C_5H_4), 65.04 (brs, C of C_5H_4), 67.07 (brm, *ipso*-C of $C_5H_4^{PPh2}$), 70.07 (brs, C of C_5H_4), 116.62 (s, *ipso*-C of $C_5H_4^{NMe2}$). ^{31}P{^{1}H} NMR (Toluene-d_8): δ −16.2 (brm, *P*Ph). MS (ESI) 968 [M + 1] for $[C_{48}H_{48}ClFe_2N_2P_2Pd]^+$. Anal. Calcd for $C_{48}H_{48}Cl_2Fe_2N_2P_2Pd$: C, 57.43; H, 4.82; N, 2.79. Found: C, 57.59; H, 5.03; N, 2.89.

Reactions of AgSbF$_6$ with Fc′(PMes$_2$)(P^{t}Bu$_2$)·PdCl$_2$ (8), and [Fc′(NMe$_2$)(PPh$_2$)]$_2$·PdCl$_2$ (9)

Solid $AgSbF_6$ (0.1 mmol, 0.034 g) was added into a DCM solution (20 mL) of Fc′(PMes$_2$)(P^{t}Bu$_2$)·PdCl$_2$ (0.1 mmol) or [Fc′(NMe$_2$)(PPh$_2$)]$_2$·PdCl$_2$ (individually 0.1 and 0.05 mmol for selectively synthesizing **11** and **12**, respectively). After stirring for overnight at rt., the solution was filtered through a PTFE

syringe filter and the product was crystallized by diffusion with hexanes and washed with multiple times of pentanes (3 × 20 mL).

[Fc′(PMes$_2$)(P^{t}Bu$_2$)·PdCl][SbF$_6$] (10)

Yield 93%. ^{1}H NMR (CD_2Cl_2): δ 1.58 (d, 18H, P–C-(CH_3)$_3$, J = 16 Hz), 2.28 (s, 6H, *p*-CH_3 of Mes), 2.59 (s, 6H, *o*-CH_3 of Mes), 4.00 (m, 2H, H of $C_5H_4^{PMes2}$), 4.46 (m, 2H, H of $C_5H_4^{PMes2}$), 5.40 (m, 2H, H of $C_5H_4^{PPh2}$), 5.57 (m, 2H, H of $C_5H_4^{PPh2}$), 6.95 (d, 4H, *m*-*H* of Mes, J = 4 Hz). ^{13}C NMR (CD_2Cl_2): δ 21.12 (s, *p*-*C*H$_3$ of Mes), 24.66 (d, *o*-*C*H$_3$ of Mes, J = 8 Hz), 31.55 (s, P–C-(*C*H$_3$)$_3$), 38.17 (dd, P–*C*-(CH$_3$)$_3$, J = 12 and 5 Hz), 72.07 (d, C of C_5H_4, J = 7 Hz), 72.23 (d, C of C_5H_4, J = 11 Hz), 82.71 (d, C of C_5H_4, J = 6 Hz), 83.31 (d, C of C_5H_4, J = 6 Hz), 131.63 (d, *m*-C of Mes, J = 9 Hz), 142.95 (d, C of Ph, J = 3 Hz), 143.49 (dd, C of Ph, J = 11 and 2 Hz). ^{31}P {^{1}H} NMR (CD_2Cl_2): δ 26.0 (d, *P*^{t}Bu, J = 425 Hz), −47.8 (d, *P*Mes, J = 425 Hz). ^{19}F NMR (CD_2Cl_2): −134.2 to −111.3 (brm, SbF_6). MS (ESI) 740 [M] for $[C_{36}H_{48}ClFeP_2Pd]^+$. Anal. Calcd for $C_{36}H_{48}ClF_6FeP_2PdSb$: C, 44.29; H, 4.96. Found: C, 44.53; H, 4.63.

[Fc′(NMe$_2$)(PPh$_2$)·PdCl][SbF$_6$] (11)

Yield 51%. ^{1}H NMR (CD_2Cl_2): δ 3.06 (d, 6H, NCH_3, J = 4 Hz), 3.38 (s, 2H, H of $C_5H_4^{PPh2}$), 3.45 (s, 2H, H of $C_5H_4^{PPh2}$), 5.83 (s, 2H, H of $C_5H_4^{PPh2}$), 5.99 (s, 2H, H of $C_5H_4^{PPh2}$), 7.54–7.56 (brm, 4H, aryl-H^{Ph}), 7.63 (d, 2H, aryl-H^{Ph}, J = 7 Hz), 8.15 (dd, 4H, aryl-H^{Ph}, J = 13, 8 Hz). ^{13}C NMR (CD_2Cl_2): δ 45.72 (d, N*C*H$_3$, J = 3 Hz), 60.41 (s, C of $C_5H_4^{NMe2}$), 73.98 (d, C of $C_5H_4^{PPh2}$, J = 11 Hz), 80.40 (s, C of $C_5H_4^{NMe2}$), 87.75 (d, C of $C_5H_4^{PPh2}$, J = 8 Hz), 123.29 (d, *ipso*-C of Ph, J = 63 Hz), 130.00 (d, aryl-C of Ph, J = 13 Hz), 133.79 (d, aryl-C of Ph, J = 3 Hz), 135.49 (d, aryl-C of Ph, J = 13 Hz). ^{19}F NMR (CD_2Cl_2): −111.3 (brs, SbF_6). ^{31}P{^{1}H} NMR (CD_2Cl_2): δ 1.2 (brs). *Note*: As compound **11** contains substantial amount of impurities, which could not be removed by multiple crystallization attempts, CHN measurements produced non-reproducible results. High resolution mass measurement (ESI) from this complex showed peak for cation $[C_{24}H_{24}ClFeNPPd]^+$ at 553.9739 (calculated exact mass is 553.9719).

[Fc′(NMe$_2$)(PPh$_2$)·PdPPh$_2$(C$_5$H$_5$)][SbF$_6$]$_2$ (12)

Yield *ca.* 32% on the basis of starting [Fc′(NMe$_2$)(PPh$_2$)]$_2$·PdCl$_2$. ^{1}H NMR (CD_2Cl_2): δ 2.51 (brm, 6H, NCH_3), 3.38 (m, 2H, H of $C_5H_4^{PPh2}$), 3.44 (pst, 2H, H of $C_5H_4^{PPh2}$), 5.76 (pst, 2H, H of $C_5H_4^{NMe2}$), 5.93 (d, 2H, H of $C_5H_4^{NMe2}$, J = 2 Hz), 7.48 (brs, 5H, aryl-H^{Ph}), 7.56 (td, 4H, aryl-H^{Ph}, J = 8 and 3 Hz), 7.63 (dd, 4H, aryl-H^{Ph}, J = 9 and 7 Hz), 8.15 (dd, 4H, aryl-H^{Ph}, J = 13 and 8 Hz). ^{13}C NMR (CD_2Cl_2): δ 45.75 (d, N*C*H$_3$, J = 3 Hz), 60.41 (s, C of $C_5H_4^{NMe2}$), 74.00 (d, C of $C_5H_4^{PPh2}$, J = 11 Hz), 80.36 (s, C of $C_5H_4^{NMe2}$), 87.71 (d, C of $C_5H_4^{PPh2}$, J = 8 Hz), 130.03 (d, aryl-C of PPh^{C5H4}, J = 13 Hz), 133.83 (d, aryl-C of PPh^{C5H4}, J = 3 Hz), 135.52 (d, aryl-C of PPh^{C5H4}, J = 13 Hz). ^{19}F NMR (CD_2Cl_2): −120.6 (brs, SbF_6). ^{31}P{^{1}H} NMR (CD_2Cl_2): δ −5.6 (d, *P*Ph$_2^{Fc}$, J = 37 Hz), 20.6 (d, *P*Ph$_2$C$_5$H$_4$, J = 37 Hz). *Note*: As compound **12** contains substantial amount of impurities, which could not be removed by multiple crystallization attempts, CHN measurements produced non-reproducible results. High resolution mass measurement (MALDI) from this complex showed [M + 2] peak for cation $[C_{41}H_{39}F_6FeNP_2PdSb]^+$ (or [Fc′(PPh$_2$)(NMe$_2$)·Pd(PC$_5$H$_4$Ph$_2$)]$^+$(SbF_6)$^-$, calculated exact mass for M + 2 is 1005.9884) at 1006.0550 and $[C_{48}H_{48}F_6Fe_2N_2P_2PdSb]^+$ (or [Fc′(PPh$_2$)(NMe$_2$)·Pd(PPh$_2$)Fc′(NMe$_2$)]$^+$(SbF_6)$^-$, calculated exact mass is 1166.9969) at 1167.1100. This result supports our speculation of [Fc′(PPh$_2$)(NMe$_2$)·Pd(PPh$_2$)Fc′(NMe$_2$)]$^+$(SbF_6)$^-$ being an intermediate in the formation of compound **12**.

[Fc′(NMe$_2$)(PPh$_2$)·PdPPh$_3$][BF$_4$]$_2$ (13)

A DCM solution (15 mL) of PPh$_3$ (0.039 g, 0.15 mmol) was added dropwise to another DCM solution (15 mL) of Fc′(NMe$_2$)(PPh$_2$) (0.062 g, 0.15 mmol) and [Pd(MeCN)$_4$][BF$_4$]$_2$ (0.067 g, 0.15 mmol). After stirring at room temperature for 2 h the color of the reaction mixture changes from bluish green to dark red. All the volatiles were removed in high vacuum (10^{-3} mbar) and further extracted with DCM (15 mL) and crystalized *via* slow diffusion of hexanes at room temperature. Crystallized yield *ca.* 97%. ^{1}H NMR (CD_2Cl_2): δ 2.46 (brs, 6H, NCH_3), 3.74 (brs, 2H, H of $C_5H_4^{PPh2}$), 4.28 (brs, 2H, H of $C_5H_4^{PPh2}$), 5.59 (brs, 2H, H of $C_5H_4^{NMe2}$), 5.74 (brs, 2H, H of $C_5H_4^{NMe2}$), 7.45 (m, 10H, aryl-H of Ph), 7.53–7.65 (m, 15H, aryl-H of Ph). ^{13}C NMR (CD_2Cl_2): δ 48.49 (s, N*C*H$_3$), 61.87 (d, C of $C_5H_4^{NMe2}$, J = 2 Hz), 73.67 (d, C of $C_5H_4^{PPh2}$, J = 11 Hz), 80.98 (s, C of $C_5H_4^{NMe2}$), 87.66 (d, C of $C_5H_4^{PPh2}$, J = 9 Hz), 102.35 (d, *ipso*-C of $C_5H_4^{NMe2}$, J = 4 Hz), 119.43 (d, *ipso*-C of $C_5H_4^{PPh2}$, J = 65 Hz), 128.49 (d, *ipso*-C of Ph, J = 48 Hz), 130.15 (d, aryl-C of Ph, J = 13 Hz), 130.20 (d, aryl-C of Ph, J = 11 Hz), 133.01 (d, aryl-C of Ph, J = 3 Hz), 133.89 (d, aryl-C of PPh, J = 3 Hz), 134.89 (d, aryl-C of Ph, J = 12 Hz), 135.54 (d, aryl-C of PPh^{Fc}, J = 12 Hz). ^{11}B NMR (CD_2Cl_2): δ −1.2 (s, *B*F$_4$). ^{19}F NMR (CD_2Cl_2): δ −151.0 (s, B*F*$_4$). ^{31}P {^{1}H} NMR (CD_2Cl_2): δ −4.7 (d, *P*Ph$_2^{Fc}$, J = 36 Hz), 21.1 (d, *P*Ph$_3$, J = 36 Hz). MS (ESI) 869 [M] for $[C_{42}H_{39}BF_4FeNP_2Pd]^+$. Anal. Calcd for $C_{43}H_{41}B_2Cl_2F_8FeNP_2Pd$ (**13**·CH_2Cl_2): C, 49.64; H, 3.97; N, 1.35. Found: C, 49.61; H, 4.14; N, 1.48.

[Fc′(PPh$_2$)(NMe$_2$)·Pd(PPh$_2$)Fc′(NMe$_2$)][BF$_4$]$_2$ (14)

A DCM solution (15 mL) of PR$_3$ (R = *o*-tollyl or Mes, 0.15 mmol) was added dropwise to another DCM solution (15 mL) of Fc′(NMe$_2$)(PPh$_2$) (0.15 mmol) and [Pd(MeCN)$_4$][BF$_4$]$_2$ (0.066 g, 0.15 mmol). After stirring at room temperature for 16 h, all the volatiles were removed in high vacuum (10^{-3} mbar) and further extracted with DCM (15 mL) and crystalized *via* slow diffusion of hexanes at room temperature. Crystals were thoroughly washed with toluene (3 × 10 mL), ether (3 × 10 mL) and pentane (2 × 10 mL) before characterization. Crystallized yield: 56%. ^{1}H NMR (CD_2Cl_2): δ 2.48 (s, 6H, NCH_3^{Int}), 3.14 (brs, 6H, NCH_3^{Ext}), 3.58 (brs, 2H, H of $C_5H_4^{Ext}$), 3.71 (brs, 2H, H of $C_5H_4^{Int}$), 4.11 (brs, 2H, H of $C_5H_4^{Int}$), 4.54 (brs, 2H, H of $C_5H_4^{Ext}$), 4.72 (brs, 2H, H of $C_5H_4^{Int}$), 4.75 (brs, 2H, H of $C_5H_4^{Ext}$), 5.53 (brs, 2H, H of $C_5H_4^{Int}$), 5.70 (brs, 2H, H of $C_5H_4^{Int}$), 7.46–7.54 (brm, 8H, H of Ph^{Int}), 7.60–7.65 (brm, 8H, H of Ph^{Ext}), 7.85–7.89 (brdd, 4H, H of Ph^{Int} & Ph^{Ext}). ^{31}P {^{1}H} NMR (CD_2Cl_2): δ −3.4 (d, *P*Ph$_2^{Int}$, J = 36 Hz), 20.3 (d, *P*Ph$_2^{Ext}$, J = 36 Hz) (Fig. S43‡); −2.4 (d, *P*Ph$_2^{Int}$, J = 36 Hz), 21.6

(d, $P\mathrm{Ph}_2^{\mathrm{Ext}}$, J = 36 Hz) (Fig. S45‡). ^{31}P NMR (CD_2Cl_2): δ −5.5 (brs, $P\mathrm{Ph}_2^{\mathrm{Int}}$), −18.3 (brs, $P\mathrm{Ph}_2^{\mathrm{Ext}}$) (Fig. S44‡). ^{11}B NMR (CD_2Cl_2): δ −1.12 (s, BF_4) (Fig. S44‡). ^{19}F NMR (CD_2Cl_2): δ −151.11 (brs, BF_4). HRMS (MALDI) 932.0970 and 769.0980 [M] for $[C_{41}H_{39}FeNP_2Pd]^{2+}$ and $[C_{24}H_{24}FeNP_2Pd]^{2+}$ (for sample showed in Fig. S43 and S44 of ESI‡). Anal. Calcd for $C_{48}H_{48}B_2F_8Fe_2N_2P_2Pd$: C, 52.10; H, 4.37; N, 2.53. Found: C, 51.65; H, 4.44; N, 2.45 (for sample showed in Fig. S44 of ESI‡) and C, 50.09; H, 4.04; N, 2.50 (for sample showed in Fig. S43 of ESI‡). *Note*: The azaphosphaferrocene unit, which contains both the N-Pd and P-Pd bonds, has been termed as "Internal" (in short "Int"), whereas similar unit, which contains only P-Pd bond, has been termed as "External" (in short "Ext"). Compound **14** can also be synthesized (yield 73%) by reacting **3a** with 0.5 eq. of $[Pd(MeCN)_4][BF_4]_2$ (Fig. S45 of ESI‡; Anal. found: C, 51.89; H, 4.62; N, 2.45, Anal. Calcd for $C_{48}H_{48}B_2F_8Fe_2N_2P_2Pd$: C, 52.10; H, 4.37; N, 2.53).

$[Fc'(PPh_2)(NMe_2)\cdot PdP(p\text{-}OMe\text{-}C_6H_4)_3][BF_4]_2$ (15)

An acetone solution (15 mL) of $[Fc'(NMe_2)(PPh_2)][PdPPh_3][BF_4]_2$ (**13**, 0.143 g, 0.15 mmol) was added to another suspension of $P(p\text{-}OMe\text{-}C_6H_4)_3$ (0.053 g, 0.015 mmol) in acetone (15 mL). The reaction mixture was stirred for 10 min at room temperature and subsequently heated at 50 °C for 40 h. The progress of the reaction was monitored by ^{31}P NMR and all the volatiles were removed when no starting material peaks were observed (Fig. S50–S52, ESI‡). Crystallized yield (57%) was obtained by slow diffusion of hexanes in the solution of DCM. To remove all the residual phosphines, the crystals were thoroughly washed with Et_2O (4 × 20 mL) before characterization. ^{1}H NMR (CD_2Cl_2): δ 2.49 (d, 6H, NCH_3, J = 3.7 Hz), 3.74 (s, 2H, H of C_5H_4), 3.82 (s, 9H, OCH_3), 4.27 (pst, 2H, H of C_5H_4), 5.53 (pst, 2H, H of C_5H_4), 5.70 (s, 2H, H of C_5H_4), 6.93 (m, 6H, *m*-H of Ph^{OMe}), 7.46 (td, 6H, *o*-H of Ph^{OMe}, J = 7.8, 3.1 Hz,), 7.51–7.59 (m, 10H, H of Ph). ^{13}C NMR (CD_2Cl_2): δ 48.57 (s, NCH_3), 56.04 (s, OCH_3), 61.66 (d, C of $C_5H_4^{NMe2}$, J = 2 Hz), 73.35 (d, C of $C_5H_4^{PPh2}$, J = 11 Hz), 80.31 (s, C of $C_5H_4^{NMe2}$), 86.99 (d, C of $C_5H_4^{PPh2}$, J = 9 Hz), 102.04 (d, *ipso*-C of $C_5H_4^{NMe2}$, J = 4 Hz), 115.64 (d, aryl-C of Ph^{OMe}, J = 12.5 Hz), 119.67 (dm, *ipso*-C of PPh^{Fc}, J = 55 Hz), 119.87 (dd, *ipso*-C of Ph^{OMe}, J = 64, 4 Hz), 130.09 (d, aryl-C of Ph^{OMe}, J = 13 Hz), 133.77 (d, aryl-C of PPh^{Fc}, J = 3 Hz), 135.49 (d, aryl-C of PPh^{Fc}, J = 12 Hz), 136.42 (d, aryl-C of PPh^{Fc}, J = 13.1 Hz), 163.32 (d, *p*-C of Ph^{OMe}, J = 3 Hz). ^{31}P $\{^1H\}$ NMR (CD_2Cl_2): δ −4.9 (d, $P\mathrm{Ph}_2$, J = 32 Hz), 19.9 (d, $P(p\text{-}OMe\text{-}C_6H_4)_3$, J = 32 Hz). ^{11}B NMR (CD_2Cl_2): δ −1.2 (s, BF_4). ^{19}F NMR (CD_2Cl_2): δ −151.3 (s, BF_4). MS (ESI) 959 [M] for $[C_{45}H_{45}BF_4FeNO_3P_2Pd]^+$. Anal. Calcd for $C_{45}H_{45}B_2F_8FeNO_3P_2Pd$: C, 51.69; H, 4.34; N, 1.34. Found: C, 51.67; H, 4.64; N, 1.30.

Conclusions

Coordination of $PdCl_2$ with a set of P,N and P,P ligands with 1,1′-ferrocenylene backbone has been explored. While for the P,N ligand monodentate binding was observed, the P,P ligands coordinated in bidentate fashion to the palladium atom. Chloride abstraction led to cationic Pd complexes with bidentate ligand coordination involving Fe → Pd interaction. With P, P ligand **8** this Fe–Pd distance in complex **10** was found shortest as compared to analogous previously published bisphosphane complexes. In the same vein, with P,N ligand **3a**, the Fe–Pd distance in complex **11** was also shortest compared with analogous previously published complexes containing ferrocene bridged P,N ligands. By contrast, the same ligand **3a** is also involved in the longest Fe–Pd distances observed for the here reported dicationic Pd complexes **12–15**, as compared to those reported for complexes of analogous P,N ligands. The Fe–Pd distances were found to be determined primarily by the distances between the ferrocene moieties and the P–Pd–P/N scaffolds, and secondarily by a complex counterbalance of steric and molecular distortions. These structural trends were corroborated by DFT calculations which furthermore indicated a very shallow minimum on the potential energy surface. The stretching of the Fe–Pd bond can be easily counterbalanced by steric effects and secondary interactions. Consistent with these findings, CV measurements demonstrated that reversible iron centered oxidation, which was possible for the free ligand, is suspended by the Fe → Pd interaction.

Author contributions

Supervision, writing and resources, R.P. and Z.K.; conceptualization, syntheses and characterization of all compounds, writing, and visualization, S.D.; electrochemical characterization, F.R., crystallographic structure optimization, C.B.; theoretical calculations, Z.K. All authors have read and agreed to the published version of the manuscript.

Conflicts of interest

Authors declare no conflicts to interest for this report.

Acknowledgements

The authors would like to thank the ZFF Program for financial support. Z. K. is grateful for the general support of János Bolyai Research Scholarship, Project UNKP-22-5-BME-298 and TKP2021-EGA-02 provided by the Ministry of Innovation and Technology of Hungary.

References

1 P. Štěpnička, Ferrocene Chemistry, *Eur. J. Inorg. Chem.*, 2022, **2022**, e202200388.
2 P. Stepnicka, Forever young: the first seventy years of ferrocene, *Dalton Trans.*, 2022, **51**, 8085–8102.
3 D. E. Herbert, U. F. Mayer and I. Manners, Strained metallocenophanes and related organometallic rings contain-

ing pi-hydrocarbon ligands and transition-metal centers, *Angew. Chem., Int. Ed.*, 2007, **46**, 5060–5081.
4 V. Bellas and M. Rehahn, Polyferrocenylsilane-based polymer systems, *Angew. Chem., Int. Ed.*, 2007, **46**, 5082–5104.
5 A. Alkan, L. Thomi, T. Gleede and F. R. Wurm, Vinyl ferrocenyl glycidyl ether: an unprotected orthogonal ferrocene monomer for anionic and radical polymerization, *Polym. Chem.*, 2015, **6**, 3617–3624.
6 R. Pietschnig, Polymers with pendant ferrocenes, *Chem. Soc. Rev.*, 2016, **45**, 5216–5231.
7 L. Cao, I. Manners and M. A. Winnik, Influence of the interplay of crystallization and chain stretching on micellar morphologies: Solution self-assembly of coil-crystalline poly(isoprene-block-ferrocenylsilane), *Macromolecules*, 2002, **35**, 8258–8260.
8 F. Jäkle, M. Gallei and H. Qiu, 30 Year anniversary of polyferrocenylsilanes: An inspiration for new advances in main group and transition metal-containing polymers, *Polymer*, 2022, **254**, 125062.
9 S. Dey, D. Kargin, M. V. Höfler, B. Szathmári, C. Bruhn, T. Gutmann, Z. Kelemen and R. Pietschnig, Oligo- and polymerization of phospha [2]ferrocenophanes to one dimensional phosphorus chains with ferrocenylene handles, *Polymer*, 2022, **242**, 124589.
10 B. Bagh, N. C. Breit, S. Dey, J. B. Gilroy, G. Schatte, K. Harms and J. Muller, Cyclic and linear polyferrocenes with silicon and tin as alternating bridges, *Chemistry*, 2012, **18**, 9722–9733.
11 M. Saleem, H. Yu, L. Wang, Z. ul Abdin, H. Khalid, M. Akram, N. M. Abbasi and J. Huang, Review on synthesis of ferrocene-based redox polymers and derivatives and their application in glucose sensing, *Anal. Chim. Acta*, 2015, **876**, 9–25.
12 X. Sui, X. Feng, M. A. Hempenius and G. J. Vancso, Redox active gels: synthesis, structures and applications, *J. Mater. Chem. B*, 2013, **1**, 1658.
13 J. Elbert, J. Mersini, N. Vilbrandt, C. Lederle, M. Kraska, M. Gallei, B. Stühn, H. Plenio and M. Rehahn, Reversible Activity Modulation of Surface-Attached Grubbs Second Generation Type Catalysts Using Redox-Responsive Polymers, *Macromolecules*, 2013, **46**, 4255–4267.
14 C. Ornelas, Application of ferrocene and its derivatives in cancer research, *New J. Chem.*, 2011, **35**, 1973.
15 G. Jaouen, A. Vessieres and S. Top, Ferrocifen type anti cancer drugs, *Chem. Soc. Rev.*, 2015, **44**, 8802–8817.
16 R. L. Hailes, A. M. Oliver, J. Gwyther, G. R. Whittell and I. Manners, Polyferrocenylsilanes: synthesis, properties, and applications, *Chem. Soc. Rev.*, 2016, **45**, 5358–5407.
17 S. Takahashi and J. I. Anzai, Recent Progress in Ferrocene-Modified Thin Films and Nanoparticles for Biosensors, *Materials*, 2013, **6**, 5742–5762.
18 P. Debroy and S. Roy, Recent advances in the synthesis and properties of ferrocenes having an unsaturated backbone, *Coord. Chem. Rev.*, 2007, **251**, 203–221.
19 D. P. Puzzo, A. C. Arsenault, I. Manners and G. A. Ozin, Electroactive inverse opal: a single material for all colors, *Angew. Chem., Int. Ed.*, 2009, **48**, 943–947.
20 D. Löber, S. Dey, B. Kaban, F. Roesler, M. Maurer, H. Hillmer and R. Pietschnig, 3D Micro/Nanopatterning of a Vinylferrocene Copolymer, *Molecules*, 2020, **25**, 2438.
21 K.-S. Gan and T. S. A. Hor, in *Ferrocenes: Homogeneous Catalysis, Organic Synthesis, Materials Science*, ed. A. Togni and T. Hayashi, John Wiley & Sons, 2007, ch. 1, pp. 3–104.
22 S. W. Chien and T. S. A. Hor, in *Ferrocenes: Ligands, Materials and Biomolecules*, ed. A. Togni and T. Hayashi, John Wiley & Sons, 2008, ch. 2, pp. 33–116.
23 S. Dey and R. Pietschnig, Chemistry of sterically demanding dppf-analogs, *Coord. Chem. Rev.*, 2021, **437**, 213850.
24 J. Schulz, J. Antala, I. Cisarova and P. Stepnicka, Beyond phosphorus: synthesis, reactivity, coordination behaviour and catalytic properties of 1,1′-bis(diphenylstibino)ferrocene, *Dalton Trans.*, 2023, **52**, 1198–1211.
25 P. Vosáhlo and P. Štěpnička, Assessing the role of substituents in ferrocene acylphosphines and their impact on gold-catalysed reactions, *New J. Chem.*, 2023, **47**, 4510–4520.
26 A. Fihri, P. Meunier and J.-C. Hierso, Performances of symmetrical achiral ferrocenylphosphine ligands in palladium-catalyzed cross-coupling reactions: A review of syntheses, catalytic applications and structural properties, *Coord. Chem. Rev.*, 2007, **251**, 2017–2055.
27 T. J. Colacot and S. Parisel, in *Ferrocenes: Ligands, Materials and Biomolecules*, ed. P. Štěpnička, John Wiley & Sons, 2008, ch. 3, pp. 117–140.
28 G. Bandoli and A. Dolmella, Ligating ability of 1,1′-bis (diphenylphosphino)ferrocene: a structural survey (1994–1998), *Coord. Chem. Rev.*, 2000, **209**, 161–196.
29 M. N. Birkholz, Z. Freixa and P. W. van Leeuwen, Bite angle effects of diphosphines in C-C and C-X bond forming cross coupling reactions, *Chem. Soc. Rev.*, 2009, **38**, 1099–1118.
30 P. Dierkes and P. W. N. M. van Leeuwen, The bite angle makes the difference: a practical ligand parameter for diphosphine ligands, *J. Chem. Soc., Dalton Trans.*, 1999, 1519–1529.
31 P. W. N. M. van Leeuwen, P. C. J. Kamer and J. N. H. Reek, The bite angle makes the catalyst, *Pure Appl. Chem.*, 1999, **71**, 1443–1452.
32 P. Vosáhlo, I. Císařová and P. Štěpnička, Comparing the asymmetric dppf-type ligands with their semi-homologous counterparts, *J. Organomet. Chem.*, 2018, **860**, 14–29.
33 K. Skoch, I. Cisarova, J. Schulz, U. Siemeling and P. Stepnicka, Synthesis and characterization of 1′-(diphenylphosphino)-1-isocyanoferrocene, an organometallic ligand combining two different soft donor moieties, and its Group 11 metal complexes, *Dalton Trans.*, 2017, **46**, 10339–10354.
34 P. Štěpnička, in *Ferrocenes: Ligands, Materials and Biomolecules*, ed. P. Štěpnička, John Wiley & Sons, 2008, ch. 5, pp. 177–204.

35 H.-U. Blaser, W. Chen, F. Camponovo and A. Togni, in *Ferrocenes: Ligands, Materials and Biomolecules*, ed. P. Štěpnička, John Wiley & Sons, 2008, ch. 6, pp. 205–235.
36 P. Štěpnička and M. Lamač, in *Ferrocenes: Ligands, Materials and Biomolecules*, ed. P. Štěpnička, John Wiley & Sons, 2008, ch. 7, pp. 237–277.
37 U. Siemeling, in *Ferrocenes: Ligands, Materials and Biomolecules*, ed. P. Štěpnička, John Wiley & Sons, 2008, ch. 4, pp. 141–176.
38 A. L. Boyes, I. R. Butler and S. C. Quayle, Palladium(II) complexes of (diisopropylphosphino)-ferrocenes: improved catalysts for the Heck reaction, *Tetrahedron Lett.*, 1998, **39**, 7763–7766.
39 W. R. Cullen, T. J. Kim, F. W. B. Einstein and T. Jones, Structure of the hydrogenation catalyst [(PP)Rh(NBD)] ClO_4, PP = $(\eta^5\text{-}(Me_3C)_2PC_5H_4)_2Fe$, and some comparative rate studies, *Organometallics*, 1983, **2**, 714–719.
40 B. C. Hamann and J. F. Hartwig, Systematic Variation of Bidentate Ligands Used in Aryl Halide Amination. Unexpected Effects of Steric, Electronic, and Geometric Perturbations, *J. Am. Chem. Soc.*, 1998, **120**, 3694–3703.
41 O. V. Gusev, T. y. A. Peganova, A. M. Kalsin, N. V. Vologdin, P. V. Petrovskii, K. A. Lyssenko, A. V. Tsvetkov and I. P. Beletskaya, Palladium Complexes with Metallocene-Bridged Bidentate Diphosphine Ligands: Synthesis, Structure, and Catalytic Activity in Amination and Cross-Coupling Reactions, *Organometallics*, 2006, **25**, 2750–2760.
42 I. R. Butler, W. R. Cullen, T. J. Kim, S. J. Rettig and J. Trotter, 1,1′-Bis(alkylarylphosphino)ferrocenes: synthesis, metal complex formation, and crystal structure of three metal complexes of $Fe(\eta^5\text{-}C_5H_4PPh_2)_2$, *Organometallics*, 1985, **4**, 972–980.
43 T.-Y. Dong and C.-K. Chang, A Novel Convenient Method to Synthesize Unsymmetrical 1,1′-Disubstituted Ferrocenes Consisting of Various Phosphino, Thiolato and Pyridyl Substituents, *J. Chin. Chem. Soc.*, 1998, **45**, 577–579.
44 L. E. Hagopian, A. N. Campbell, J. A. Golen, A. L. Rheingold and C. Nataro, Synthesis and electrochemistry of late transition metal complexes containing 1,1′-bis(dicyclohexylphosphino)ferrocene (dcpf). The X-ray structure of $[PdCl_2(dcpf)]$ and Buchwald–Hartwig catalysis using $[PdCl_2(bisphosphinometallocene)]$ precursors, *J. Organomet. Chem.*, 2006, **691**, 4890–4900.
45 A. Fihri, J.-C. Hierso, A. Vion, D. H. Nguyen, M. Urrutigoïty, P. Kalck, R. Amardeil and P. Meunier, Diphosphines of dppf-Type Incorporating Electron-Withdrawing Furyl Moieties Substantially Improve the Palladium-Catalysed Amination of Allyl Acetates, *Adv. Synth. Catal.*, 2005, **347**, 1198–1202.
46 M. Yamashita, J. V. C. Vicario and J. F. Hartwig, Trans Influence on the Rate of Reductive Elimination. Reductive Elimination of Amines from Isomeric Arylpalladium Amides with Unsymmetrical Coordination Spheres, *J. Am. Chem. Soc.*, 2003, **125**, 16347–16360.
47 J.-C. Hierso, F. Lacassin, R. Broussier, R. Amardeil and P. Meunier, Synthesis and characterisation of a new class of phosphine-phosphonite ferrocenediyl dinuclear rhodium complexes, *J. Organomet. Chem.*, 2004, **689**, 766–769.
48 M. Laly, R. Broussier and B. Gautheron, Ferrocene-based phosphonite–phosphine ligands, Pd and Rh complexes, *Tetrahedron Lett.*, 2000, **41**, 1183–1185.
49 P. Štěpnička and I. Císařová, Synthesis of [1′-(diphenylthiophosphoryl)ferrocenyl]ethyne and alkyne-metal complexes thereof, *J. Organomet. Chem.*, 2006, **691**, 2863–2871.
50 M. E. Wright, 1,1′-Bis(tri-*n*-butylstannyl)ferrocene: selective transmetalation applied to the synthesis of new ferrocenyl ligands, *Organometallics*, 1990, **9**, 853–856.
51 J. Podlaha, P. Štěpnička, J. Ludvík and I. Císařová, 1′-(Diphenylphosphino)ferrocenecarboxylic Acid and Its P-Oxide and Methyl Ester: Synthesis, Characterization, Crystal Structure, and Electrochemistry, *Organometallics*, 1996, **15**, 543–550.
52 L. Meca, D. Dvořák, J. Ludvík, I. Císařová and P. Štěpnička, Synthesis, Structures, and Electrochemistry of Group 6 Aminocarbenes with a P-Chelating 1′-(Diphenylphosphino)ferrocenyl Substituent, *Organometallics*, 2004, **23**, 2541–2551.
53 I. R. Butler, S. J. Coles, M. B. Hursthouse, D. J. Roberts and N. Fujimoto, Ferrocene-based ligands in ruthenium alkylidene chemistry, *Inorg. Chem. Commun.*, 2003, **6**, 760–762.
54 K. Skoch, I. Cisarova, F. Uhlik and P. Stepnicka, Comparing the reactivity of isomeric phosphinoferrocene nitrile and isocyanide in Pd(ii) complexes: synthesis of simple coordination compounds vs. preparation of P-chelated insertion products and Fischer-type carbenes, *Dalton Trans.*, 2018, **47**, 16082–16101.
55 V. C. Gibson, N. J. Long, A. J. P. White, C. K. Williams and D. J. Williams, The Synthesis and Metal Coordination Chemistry of a Novel Phosphine- and Thiolate-Substituted Ferrocenediyl Ligand, *Organometallics*, 2002, **21**, 770–772.
56 W. Zhang, Y.-i. Yoneda, T. Kida, Y. Nakatsuji and I. Ikeda, Novel chiral P,N-ferrocene ligands in palladium-catalyzed asymmetric allylic alkylations[1], *Tetrahedron: Asymmetry*, 1998, **9**, 3371–3380.
57 P. Štěpnička, I. Císařová and R. Gyepes, Synthesis and Structural Characterisation of Palladium and Group-12 Metal Complexes with a Hybrid Phosphanylphosphonate Ferrocene Ligand, *Eur. J. Inorg. Chem.*, 2006, **2006**, 926–938.
58 P. Štěpnička and I. Císařová, Synthesis, characterization and structure of rhodium(I) carbonyl complexes with O,P-chelating 1′-(diphenylphosphino)ferrocenecarboxylate or P-monodentate 1′-(diphenylphosphino)ferrocenecarboxylic acid, *J. Chem. Soc., Dalton Trans.*, 1998, 2807–2812.
59 K. Mach, J. Kubista, I. Císařová and P. Štěpnička, [μ-1κ^2O, O′:2(η^5)-Cyclopentadienylcarboxylato][2(η^5)-diphenylphosphinocyclopentadienyl]bis[1,1(η^5)-tetramethyl-

cyclopentadienyl]iron(II)titanium(III), *Acta Crystallogr., Sect. C: Cryst. Struct. Commun.*, 2002, **58**, m116–m118.

60 R. C. J. Atkinson, V. C. Gibson, N. J. Long, A. J. P. White and D. J. Williams, Synthesis, Coordination Chemistry, and Catalytic Application of a Novel Unsymmetrical P/O Ferrocenediyl Ligand, *Organometallics*, 2004, **23**, 2744–2751.

61 T. Yoshida, K. Tani, T. Yamagata, Y. Tatsuno and T. Saito, Preparation and structure of [Rh{(η^5-C_5H_4(2-C_5H_4N))(η^5-$C_5H_4PPh_2$)}(cod)]PF_6 and [Ir(H){Fe[η^5-C_5H_3(2-C_5H_4N)](η^5-$C_5H_4PPh_2$)}(cod)]PF_6; a Rh complex having a C–H···Rh interaction and a hydrido Ir complex (where cod = cycloocta-1,5-diene), *J. Chem. Soc., Chem. Commun.*, 1990, 292–294.

62 I. R. Butler, M. Kalaji, L. Nehrlich, M. Hursthouse, A. I. Karaulov and K. M. A. Malik, The palladium(II) coordination chemistry of ferrocenylphosphinobipyridines: a novel trans-chelating ligand system, *J. Chem. Soc., Chem. Commun.*, 1995, 459–460.

63 Z. Weng, S. Teo and T. S. A. Hor, Stabilization of Nickel(0) by Hemilabile P,N-Ferrocene Ligands and Their Ethylene Oligomerization Activities, *Organometallics*, 2006, **25**, 4878–4882.

64 Z. Weng, S. Teo, L. L. Koh and T. S. A. Hor, A structurally characterized Ni–Al methyl-bridged complex with catalytic ethylene oligomerization activity, *Chem. Commun.*, 2006, 1319–1321.

65 M. Widhalm, U. Nettekoven and K. Mereiter, Chiral ferrocene derivatives containing a 2,2′-bridged binaphthyl moiety, *Tetrahedron: Asymmetry*, 1999, **10**, 4369–4391.

66 O. Bárta, R. Gyepes, I. Císařová, A. Alemayehu and P. Štěpnička, Synthesis and study of Fe → Pd interactions in unsymmetric Pd(ii) complexes with phosphinoferrocene guanidine ligands, *Dalton Trans.*, 2020, **49**, 4225–4229.

67 M. Navrátil, I. Císařová and P. Štěpnička, Synthesis and coordination of hybrid phosphinoferrocenes with extended donor pendants, *Dalton Trans.*, 2022, **51**, 14618–14629.

68 Z. Weng, S. Teo, L. L. Koh and T. S. A. Hor, Ethylene Oligomerization at Coordinatively and Electronically Unsaturated Low-Valent Nickel, *Angew. Chem., Int. Ed.*, 2005, **44**, 7560–7564.

69 Z. Weng, S. Teo, L. L. Koh and T. S. A. Hor, Efficient Suzuki Coupling of Aryl Chlorides Catalyzed by Palladium(0) with a P,N Heteroligand and Isolation of Unsaturated Intermediates, *Organometallics*, 2004, **23**, 4342–4345.

70 M. Abubekerov, S. I. Khan and P. L. Diaconescu, Ferrocene-bis(phosphinimine) Nickel(II) and Palladium(II) Alkyl Complexes: Influence of the Fe–M (M = Ni and Pd) Interaction on Redox Activity and Olefin Coordination, *Organometallics*, 2017, **36**, 4394–4402.

71 K. Škoch, P. Vosáhlo, I. Císařová and P. Štěpnička, Synthesis and characterisation of Pd(ii) and Au(i) complexes with mesoionic carbene ligands bearing phosphinoferrocene substituents and isomeric carbene moieites, *Dalton Trans.*, 2020, **49**, 1011–1021.

72 M. R. Ringenberg, Beyond Common Metal–Metal Bonds, κ^3-Bis(donor)ferrocenyl → Transition-Metal Interactions, *Chem. – Eur. J.*, 2019, **25**, 2396–2406.

73 S. Dey, J. W. Quail and J. Müller, [2]Ferrocenophanes with Nitrogen in Bridging Positions, *Organometallics*, 2015, **34**, 3039–3046.

74 I. R. Butler and S. C. Quayle, The synthesis and characterisation of heterosubstituted aminoferrocenes, *J. Appl. Crystallogr.*, 1998, **552**, 63–68.

75 S. Dey, PhD Doctoral Dissertation, University of Saskatchewan, 2016.

76 H. Bhattacharjee, S. Dey, J. Zhu, W. Sun and J. Muller, Strained azabora[2]ferrocenophanes, *Chem. Commun.*, 2018, **54**, 5562–5565.

77 S. Dey, W. Sun and J. Muller, [n]Ferrocenophanes (n = 2, 3) with Nitrogen and Phosphorus in Bridging Positions, *Inorg. Chem.*, 2016, **55**, 3630–3639.

78 M. Kleoff, J. Schwan, L. Boeser, B. Hartmayer, M. Christmann, B. Sarkar and P. Heretsch, Scalable Synthesis of Functionalized Ferrocenyl Azides and Amines Enabled by Flow Chemistry, *Org. Lett.*, 2020, **22**, 902–907.

79 C. Metallinos, J. Zaifman, T. Dudding, L. Van Belle and K. Taban, Asymmetric Lithiation of Boron Trifluoride–Activated Aminoferrocenes: An Experimental and Computational Investigation, *Adv. Synth. Catal.*, 2010, **352**, 1967–1982.

80 C. Metallinos, J. Zaifman and L. Dodge, Aminoferrocene Lithiation by Boron Trifluoride Activation, *Org. Lett.*, 2008, **10**, 3527–3530.

81 M. B. Hursthouse, S. J. Coles and I. R. Butler, *CSD Commun.*, 2003, DOI: **10.5517/cc79s09**.

82 S. Dey, F. Roesler, M. V. Höfler, C. Bruhn, T. Gutmann and R. Pietschnig, Synthesis, Structure and Cu–Phenylacetylide Coordination of an Unsymmetrically Substituted Bulky dppf–Analog, *Eur. J. Inorg. Chem.*, 2021, **2022**, e202100939.

83 S. Dey, D. Buzsaki, C. Bruhn, Z. Kelemen and R. Pietschnig, Bulky 1,1′-bisphosphanoferrocenes and their coordination behaviour towards Cu(i), *Dalton Trans.*, 2020, **49**, 6668–6681.

84 G. Pilloni, B. Longato, G. Bandoli and B. Corain, Bonding ability of 1,1′-bis(diphenylthiophosphoryl)ferrocene (dptpf) and its selenium analogue towards copper(I). Crystal structure of [Cu(dptpf)]BF_4, *J. Chem. Soc., Dalton Trans.*, 1997, 819–826.

85 K. M. Gramigna, J. V. Oria, C. L. Mandell, M. A. Tiedemann, W. G. Dougherty, N. A. Piro, W. S. Kassel, B. C. Chan, P. L. Diaconescu and C. Nataro, Palladium(II) and Platinum(II) Compounds of 1,1′-Bis(phosphino)metallocene (M = Fe, Ru) Ligands with Metal–Metal Interactions, *Organometallics*, 2013, **32**, 5966–5979.

86 K. D. Cabrera, A. T. Rowland, J. M. Szarko, P. L. Diaconescu, M. W. Bezpalko, W. S. Kassel and

C. Nataro, Monodentate phosphine substitution in [Pd(κ^3-dppf)(PR_3)][BF_4]$_2$ (dppf = 1,1′-bis(diphenylphosphino)ferrocene) compounds, *Dalton Trans.*, 2017, **46**, 5702–5710.

87 M. Sato, H. Shigeta, M. Sekino and S. Akabori, Synthesis, some reactions, and molecular structure of the Pd(BF_4)2 complex of 1,1′-bis(diphenylphosphino)ferrocene, *J. Organomet. Chem.*, 1993, **458**, 199–204.

88 B. L. Blass, R. H. Sánchez, V. A. Decker, M. J. Robinson, N. A. Piro, W. S. Kassel, P. L. Diaconescu and C. Nataro, Structural, Computational, and Spectroscopic Investigation of [Pd(κ^3-1,1′-bis(di-tert-butylphosphino)ferrocenediyl)X] + (X = Cl, Br, I) Compounds, *Organometallics*, 2016, **35**, 462–470.

89 G. Mann, Q. Shelby, A. H. Roy and J. F. Hartwig, Electronic and Steric Effects on the Reductive Elimination of Diaryl Ethers from Palladium(II), *Organometallics*, 2003, **22**, 2775–2789.

90 C. F. Macrae, P. R. Edgington, P. McCabe, E. Pidcock, G. P. Shields, R. Taylor, M. Towler and J. van de Streek, Mercury: visualization and analysis of crystal structures, *J. Appl. Crystallogr.*, 2006, **39**, 453–457.

91 C. F. Macrae, I. J. Bruno, J. A. Chisholm, P. R. Edgington, P. McCabe, E. Pidcock, L. Rodriguez-Monge, R. Taylor, J. van de Streek and P. A. Wood, Mercury CSD 2.0– new features for the visualization and investigation of crystal structures, *J. Appl. Crystallogr.*, 2008, **41**, 466–470.

92 K. Jess, D. Baabe, T. Bannenberg, K. Brandhorst, M. Freytag, P. G. Jones and M. Tamm, Ni–Fe and Pd–Fe Interactions in Nickel(II) and Palladium(II) Complexes of a Ferrocene-Bridged Bis(imidazolin-2-imine) Ligand, *Inorg. Chem.*, 2015, **54**, 12032–12045.

93 S. Weller, S. H. Schlindwein, C. M. Feil, Z. Kelemen, D. Buzsáki, L. Nyulászi, S. Isenberg, R. Pietschnig, M. Nieger and D. Gudat, A Ferrocenophane-Based Diaminophosphenium Ion, *Organometallics*, 2019, **38**, 4717–4725.

94 D. Kargin, Z. Kelemen, K. Krekic, M. Maurer, C. Bruhn, L. Nyulaszi and R. Pietschnig, [3]Ferrocenophanes with the bisphosphanotetryl bridge: inorganic rings on the way to tetrylenes, *Dalton Trans.*, 2016, **45**, 2180–2189.

95 G. R. Fulmer, A. J. M. Miller, N. H. Sherden, H. E. Gottlieb, A. Nudelman, B. M. Stoltz, J. E. Bercaw and K. I. Goldberg, NMR Chemical Shifts of Trace Impurities: Common Laboratory Solvents, Organics, and Gases in Deuterated Solvents Relevant to the Organometallic Chemist, *Organometallics*, 2010, **29**, 2176–2179.

96 G. M. Sheldrick, A short history of Shelx, *Acta Crystallogr., Sect. A: Found. Crystallogr.*, 2008, **64**, 112.

97 C. F. Macrae, I. J. Bruno, J. A. Chisholm, P. R. Edgington, P. McCabe, E. Pidcock, L. Rodriguez-Monge, R. Taylor, J. van de Streek and P. A. Wood, Mercury CSD 2.0– new features for the visualization and investigation of crystal structures, *J. Appl. Crystallogr.*, 2008, **41**, 466.

98 C. F. Macrae, P. R. Edgington, P. McCabe, E. Pidcock, G. P. Shields, R. Taylor, M. Towler and J. van de Streek, Mercury: visualization and analysis of crystal structures, *J. Appl. Crystallogr.*, 2006, **39**, 453.

99 A. L. Spek, Platon Squeeze: a tool for the calculation of the disordered solvent contribution to the calculated structure factors, *Acta Crystallogr., Sect. C: Struct. Chem.*, 2015, **71**, 9.

100 I. Noviandri, K. N. Brown, D. S. Fleming, P. T. Gulyas, P. A. Lay, A. F. Masters and L. Phillips, The Decamethylferrocenium/Decamethylferrocene Redox Couple: A Superior Redox Standard to the Ferrocenium/Ferrocene Redox Couple for Studying Solvent Effects on the Thermodynamics of Electron Transfer, *J. Phys. Chem. B*, 1999, **103**, 6713.

101 P. Vosáhlo, J. Schulz, K. Škoch, I. Císařová and P. Štěpnička, Synthesis and characterisation of palladium (II) complexes with hybrid phosphinoferrocene ligands bearing additional O-donor substituents, *New J. Chem.*, 2019, **43**, 4463–4470.